NASA Technical Memorandum 80115

Some Recent Developments in the Prediction of Shock Interaction Phenomena at Hypersonic Speeds

Davis H. Crawford

OCTOBER 1979

NASA

1 Report No	2 Government Accession No	3 Recipient's Catalog No
NASA TM-80115		

4 Title and Subtitle	5 Report Date
SOME RECENT DEVELOPMENTS IN THE PREDICTION OF SHOCK INTERACTION PHENOMENA AT HYPERSONIC SPEEDS	October 1979
	6 Performing Organization Code

7 Author(s)	8 Performing Organization Report No
Davis H. Crawford	L-12669
	10 Work Unit No: 506-26-13-01

9 Performing Organization Name and Address	11 Contract or Grant No
NASA Langley Research Center Hampton, VA 23665	

12 Sponsoring Agency Name and Address	13 Type of Report and Period Covered
National Aeronautics and Space Administration Washington, DC 20546	Technical Memorandum
	14 Sponsoring Agency Code

15 Supplementary Notes

16 Abstract

The shock strengths for which either Edney type I or type II shock interference patterns can occur when two oblique shocks of opposite families intersect have been determined graphically at Mach 10 by using logarithmic-shock-polar diagrams. The theoretical region of overlap for the two types of interaction was investigated by observing in the schlieren system of the Langley 15-inch hypersonic flow apparatus the intersection of oblique shocks generated by two sharp 10° wedges as the wedge angles of attack and their relative positions were altered.

17 Key Words (Suggested by Author(s))	18 Distribution Statement
Shock interference patterns Shock–boundary-layer interaction Shock interactions	Unclassified - Unlimited Subject Category 34

19 Security Classif (of this report)	20 Security Classif (of this page)	21 No of Pages	22 Price*
Unclassified	Unclassified	38	$4.50

* For sale by the National Technical Information Service, Springfield Virginia 22161

NASA Technical Memorandum 80115

Some Recent Developments in the Prediction of Shock Interaction Phenomena at Hypersonic Speeds

Davis H. Crawford
Langley Research Center
Hampton, Virginia

National Aeronautics
and Space Administration

**Scientific and Technical
Information Branch**

1979

SUMMARY

The shock strengths for which either Edney type I or type II shock interference patterns can occur when two oblique shocks of opposite families intersect have been determined graphically at Mach 10 by using logarithmic-shock-polar diagrams. The theoretical region of overlap for the two types of interaction was investigated by observing in the schlieren system of the Langley 15-inch hypersonic flow apparatus the intersection of oblique shocks generated by two sharp 10° wedges as the wedge angles of attack and their relative positions were altered. The results from this investigation show a range of shock strengths for which either of the two interference patterns (Edney type I or type II) can exist.

INTRODUCTION

The interaction of intersecting oblique shocks of opposite families has been rigorously studied by Courant and Friedrichs (ref. 1). Two basic types of interaction systems occur, depending on the strength of the intersecting shocks. For weaker shocks the two meet and are reflected from a single point. For stronger shocks each is reflected from one of a pair of points separated by a single strong shock. These two forms of shock interaction were classified as types I and II, respectively, by Edney (ref. 2) among six types of shock interaction systems that he observed when an oblique shock intersected the bow shock of a blunt body at various locations relative to the sonic lines.

The flow conditions in a small neighborhood of the point of shock intersection may be examined graphically by using shock polars (refs. 2 and 3) or analytically (refs. 4 and 5). Graphical examination of the intersection of two oblique shocks of opposite families by use of shock polars reveals a range of shock angles at a given Mach number for which an interaction of either type I or type II might occur.

The purpose of this paper is to demonstrate the use of the graphical method of reference 3 of determining the flow conditions in the neighborhood of the point of shock intersection, to show how this method predicts the shock angle range where either type I or type II interactions can occur, and to demonstrate experimentally the two possible types of interaction occurring at the same conditions. This paper presents the logarithmic-shock-polar diagrams and the schlieren photographs for the intersection of shocks generated by a pair of wedges at Mach 10. The computed region of commonality for the two types of interference patterns is compared with that obtained experimentally.

SYMBOLS

M_n local Mach number in zones of interest (where n takes on values 1, 2, 3, . . ., 6)

M_α Mach number upstream of shock deflection (fig. 2)

M_β Mach number downstream of shock deflection (fig. 2)

p_n local stream pressure in zones of interest (where n takes on values 1, 2, 3, . . ., 6)

$p_{ns,\alpha}$ calculated local stream static pressure behind normal shock upstream of shock deflection

x horizontal distance between trailing edge of shock generator and trailing edge of body (fig. 9)

y vertical distance between trailing edge of shock generator and trailing edge of body (fig. 9)

δ_D flow deflection down; body surface deflection angle

δ_n total flow deflection in zones of interest (where n takes on values 1, 2, 3, . . ., 6)

δ_U flow deflection up; shock generator surface deflection angle

χ distance parallel to plane of longitudinal adjustment from most forward possible position of body to its test position (fig. 9)

Special notation:

①, ②, ③, ④, 3A regions in shock pattern (figs. 3, 4, and 5)

THEORETICAL DISCUSSION OF SHOCK INTERACTION

Types of Shock Interaction at a Point for Shocks of Opposite Families

Although the various types of interference patterns that can occur when two oblique shocks of different strengths intersect are well discussed in the literature (refs. 2 to 11), discussion of the two basic types is repeated here for continuity in presenting the results of this investigation.

When the intersecting shocks are so weak that their downstream velocities can be restored to a common direction by reflected shocks from a single point, the shock interaction pattern is that classified as type I by Edney (ref. 2) as shown in figure 1(a). The two weak shocks turn the uniform upstream flow into two regions of supersonic flow approaching each other obliquely. After their point of intersection, the reflected shocks must turn the flow to a common

direction along a free boundary or "contact discontinuity line," which is a shear boundary if the velocities along the boundary are unequal.

When two intersecting oblique shocks of opposite sign become so strong that the flow behind them cannot be returned to a common direction along an equilibrium pressure boundary by a pair of shocks reflected from a single point, further accommodation for the converging flows to reach a common direction is provided by two shock intersection points followed by curved boundaries which are shear layers along a region of subsonic flow. The two points of shock intersection are connected by a strong shock as shown in figure 1(b). The two point-shock interaction patterns are alike in that they are composed of a strong shock intersecting with an oblique shock and with the oblique shock reflecting from the shear layer trailing the point. This strong shock is often called the Mach reflection between these two points. The complete pattern is the simplest form of Edney's type II shock interaction.

The flow may be examined in an infinitesimal region about each of the two points in type II interaction where three shocks intersect at a point. Phenomena characteristic of this region are rigorously discussed in reference 1, where proof is offered that three shocks cannot separate the flow into three zones of continuous flow. The simplest solution for the connection of three shock fronts requires the addition of a single "contact discontinuity line" in one of the zones. This is the case with the Edney type II pattern where one portion of the gas passes through a single strong shock (Mach front) and the other portion of the gas passes through the incident shock and then through its reflection. The required "contact discontinuity line" is the shear layer separating the two portions of gas downstream of the point of shock intersection.

Logarithmic-Shock-Polar Diagram

The previously discussed three point-shock interaction patterns can be explained or predicted by a pressure-deflection-polar diagram. Use of this method to evaluate simple shock interactions is shown in reference 9 and is shown in more detail and many more applications in reference 2. However, the method shown in these references is tedious to apply because the pressure ratios are plotted on a linear scale. The ordinate distances and also the general shape of the polar for a given Mach number are a function of its vertical position on a polar diagram, thus necessitating the plotting of each separate polar when constructing a combined polar diagram. This difficulty is obviated by plotting pressure ratios to a logarithmic scale on the ordinate and flow deflections to a linear scale on the abscissa as suggested by the present author in reference 3. This choice of scales allows the preparation of a logarithmic-shock-polar family from which the pressure-deflection curves necessary for assembling a pressure-deflection polar diagram may be directly traced.

An example of such a logarithmic-shock-polar family of pressure-deflection curves is shown in figure 2. This figure contains static pressure-deflection polar diagrams for Mach numbers ranging from 1 to 20. With some interpolation, a pressure-deflection polar diagram may be traced directly from this figure for

any stream Mach number in the range shown; that is, along the solid lines (weak shock) the pressure rise across the oblique shock is shown as a function of the flow deflection. Note that the free-stream Mach number ahead of the oblique shock is constant along these lines. These static pressures are normalized with respect to the pressure behind a normal shock for convenience. The Mach number behind the oblique shock also varies with flow deflection. Points of constant downstream Mach number for the various pressure-deflection polar curves are joined by the long dashed lines. Thus the static pressure at any point on a pressure-deflection polar may be related to the next polar of interest by following either an existing or an interpolated long dashed line back to zero deflection. The solid lines of the shock polar are joined to the short dashed lines (strong shock) to complete the pressure-deflection polar diagram. Again the Mach number upstream of the oblique shock is constant along each of these lines. The logarithmic scale for the ordinate of this plot leads to the automatic multiplication of the pressure ratios with the graphical linear addition of the ordinates regardless of the vertical orientation of any particular pressure-deflection polar. As shown in reference 3, the reference pressures for successive shock polars cancel so that the final result indicated by the ordinate is the ratio of the final static pressure to the stream static pressure behind a normal shock at the initial free-stream Mach number. Thus, the logarithmic-shock-polar family chart may be used without any numerical calculations to estimate the type or possible types of interaction resulting from any combination of interacting shocks on a flight vehicle.

Application

The estimation of a resulting shock interference pattern formed by the intersection of two weak shocks of opposite sign is straightforward. The flow pattern expected with its regions of interest identified is shown in figure 3(a). The parts of the logarithmic-shock-polar family used to calculate the angles and pressures involved are shown in figure 3(b). Note that δ_1 is the flow deflection caused by the body shock, and δ_2 is the flow deflection caused by the impinging shock before the shocks intersect. The flow is thus turned from the free-stream direction to ① and to ② by the two intersecting shocks upstream of their intersection. The proper logarithmic-shock polars to be used at ① and ② to point out the direction of the equilibrium free boundary downstream of the point of shock intersection are identified in figure 2 by following the constant M_β curves from the points ① and ② to the zero deflection line of the logarithmic-shock-polar diagram. The correct placement of these properly identified polars so that their intersection ③ defines the direction and pressure of the flow downstream from the point of intersection of the shocks is illustrated in figure 3(c).

The calculation of the shock pattern formed when the shocks of opposite sign that interact are of such strength that the two converging flows cannot reach an equilibrium pressure through a single pair of trailing shocks is illustrated in figure 4. The expected shock pattern is shown in figure 4(a). The appropriate secondary polar diagrams are selected in figure 4(b), and the correct placement of the secondary polar diagrams in figure 4(c) shows that the two polars from ① and ② do not intersect, and thus a single point solution

is not possible. The pressure and flow direction downstream from the two point-shock-intersection solutions are determined in figure 4(c) at ③ and ④.

If the type I and type II shock interactions shown in figures 3(c) and 4(c) are compared, then supersonic flow is expected in figure 3(c) because the deflected streams reach equilibrium conditions before the pressure downstream from the shock interaction is high enough to support a strong shock. Conversely, figure 4(c) discloses the lack of a weak shock solution because the logarithmic-shock polars from ① and ② do not intersect. Figure 5, however, shows a similar final shock-polar diagram which suggests the possibility of either type I or type II shock interaction for the particular geometry of the interfering shock and the two-dimensional body. Type II interaction is suggested by the intersections of the polars starting from ① and ② with the strong shock part of the polar for the free-stream Mach number. The strong shock followed by the subsonic flow region is depicted by the dashed line separating the points at ③ and ④, and δ_3 and δ_4 are the angles of the shear layers following the two point-shock intersections analogous to figure 4(c). Type I interaction is suggested by the common intersection of the polars from ① and ② at a pressure level above the strong shock part of the polar from the free-stream Mach number, and δ_3 is the angle at ③A of the shear layer following this point-shock intersection analogous to ③ in figure 3(c).

Figure 5 does not indicate which shock configuration is the most stable or even suggest the circumstances where one type of interference pattern would occur in preference to the other. One logical hypothesis is that for a given flow deflection δ_1, the type I interaction would persist as the flow deflection increased past that angle where either type I or type II interaction is likely, and possibly until the polars from ① and ② failed to intersect, which would thereby preclude any chance of type I interaction. Furthermore, the type II interaction might then persist as δ_1 is reduced past the position where either interaction type I or type II is again likely, and possibly until the intersection of the polars from ① and ② occurs below the strong shock solution of the free-stream polar, thus preventing any chance of type II interaction.

The upper and lower bounds of the region where either type I or type II shock interaction may theoretically occur may be determined by using diagrams similar to figure 5 in the manner previously described. Such a procedure using a free-stream polar for Mach 10 results in the diagram shown in figure 6. This figure shows the regions where only type I shock interaction is predicted, where possibly either type I or type II shock interaction is likely, and where only type II shock interaction should occur.

EXPERIMENTAL STUDY

If the theoretical range of flow deflection angles where either an Edney type I or type II interaction could occur is correct, then several questions arise: One concerns the practical extent of this region of flow deflection

angles compared with the theoretical extent; another deals with the stability of shock interaction types I and II as they occur when either is possible. A test program was therefore conducted at Mach 10 to verify the results from the theoretical analysis.

Tunnel

The shock interference tests were performed in the Langley 15-inch hypersonic flow apparatus. This is an intermittent type of wind tunnel with a test Mach number of 10. The performance of the tunnel has previously been reported in reference 12. Since the tests of reference 12, the hypersonic flow apparatus has been reinstalled in a different location. Recent calibrations of the nozzle are in reasonable agreement with an originally published calibration. The capacities of the high-pressure source and the vacuum tanks were sufficient for running times in excess of $3\frac{1}{2}$ minutes.

The body surface deflection angle was regulated from the control room by manually operated levers which operate hydraulically driven motors to actuate the angle-of-attack sector. The position of the sector is indicated by the deflection of a galvanometer connected to the sliding contact used in a slide-wire bridge type of arrangement and positioned by the sector drive control. A special mount, which supported the body, was bolted to the sector in a position provided for this type of use.

The shapes of the flow patterns were observed and recorded by means of a single pass schlieren system. Light rays were directed through the test region and were focused upon a horizontal knife-edge which had a mirrored surface. The light beam at this focal point was split into two beams by the mirrored knife-edge, one beam forming a real image on a screen viewed by a television camera, and the other beam forming a permanent record on film.

Test Models

Details of the test models are seen in the photographs of figures 7 and 8. The shock generator and the body were wedges with sharp leading edges and a 10° included angle. Both wedges had a span of 10 cm, the body had a chord of 5 cm, and the shock generator had a chord of 10 cm. The wedges were machined of 347 stainless steel to insure dimensional stability and resistance to corrosion.

The wedges were installed in the wind tunnel as shown in the sketch of figure 9. The shock generator was mounted on the support seen in the upper part of the photograph in figure 7(b). The part shown allowed adjustment of the surface deflection angle of the shock generator. The mount was fastened to a vertical support integral with a base plate which allowed streamwise adjustment by means of screws in slotted holes. Much of this shock generator support was located in a cavity below the nozzle wall. The main part of possible tunnel airflow disturbance caused by this cavity was prevented by a fairing cover.

Test Conditions

The tests were performed in dry air at a nominal Mach number of 10. The Reynolds number based on stream conditions ahead of the wedges and on the chord of the body (5 cm) was in the range of 0.26×10^6 to 0.35×10^6. The stagnation pressure was 6.9×10^6 newtons per square meter, and the stagnation temperature varied from 480 K to 650 K. The range of surface deflection angle δ_D of the body during these tests was from 9^o to 52^o, and the surface deflection angles δ_U used for the shock generator were 12^o, 16^o, and 20^o.

Tests and Methods

Shock generator surface deflection angles were theoretically determined for which a range of body surface deflection angles might be expected to cause either type I or type II shock interaction. The shock generator surface was set at a deflection angle, and the body was rotated through a range of surface deflection angles in both directions to determine the angle where the shock interaction pattern changed either from type I to type II or from type II to type I. Data were usually taken at 1^o intervals in the surface deflection angle. Testing time was usually sufficient to determine the surface deflection angle for one interaction pattern change and then to discover the surface deflection angle when it reverted to the original pattern. Not all tests were taken in the same direction. Some tests recorded type I interaction changing to type II and reverting to type I, whereas other tests recorded the opposite order.

RESULTS AND DISCUSSION

Shock Interactions Free of Body Interference

Examples of photographic schlieren data used to determine the angles for shock interference type change from I to II and from II to I are shown in figures 10 and 11. Note that these two examples are executed in opposite order and disclose that a range of wedge positions exists where either type of shock interaction occurs. This range is observed in the form of an overlap of positions where the type I pattern persists (as the body surface deflection is increased) to an angle several degrees greater than the minimum angle where type II interaction has been observed and where the type II pattern persists (as the body surface deflection is reduced) to an angle several degrees less than the maximum angle where type I interaction has been observed. The results did not repeat exactly, but the direction of the test apparently had a negligible effect. As the surface deflection angles changed in each direction, the shock interference pattern became more unstable as the surface deflection progressed into the range where both type I and type II shock interactions were possible. The overall results verify the theoretical hypothesis.

The theoretical study showing the overlap of type I and type II shock interactions gives no hint of the extent of the strong shock, characteristic of the type II interaction, when it occurs. A reexamination of the photographs of figures 10 and 11 shows that, although the strong shock region is never of

great extent, it rather suddenly appears as the attitude is increased but disappears more evenly as the attitude is decreased.

Shock Interactions Influenced by Body Proximity

In the proximity of the body a different manner of alteration occurs when a shock pattern changes from type I to type II than when it changes from type II to type I (fig. 12). Examination of this figure discloses that the shocks trailing the initial shock intersection just miss striking the trailing edge of the body when the shock interaction is type I. When the interaction changes to type II, however, the normal shock is extensive, striking the body shock two-thirds of the body chord length ahead of the trailing edge. As the body surface deflection angle is then reduced from the value which caused type II interaction to appear, the extensive normal shock is slowly and evenly reduced in size until the last example of type II shock formation has a barely visible normal segment. The apparent region of overlap of positions where either type of interaction may occur still covers a large range of body surface deflection angles from 23° to 30°, even when the interaction point is in the proximity of the body.

When the body is moved an increment farther downstream until the trailing shock from the type I interaction strikes the trailing edge of the body, the effect of body surface deflection angles upon the shock interaction pattern is altered. A sequence of pictures showing the shock interaction patterns for this configuration is presented in figure 13. The change from type I to type II shock interaction now occurs at a lower surface deflection angle, and the region of overlap where either type I or type II shock interaction can occur has become very small. Possibly the play of the trailing shock on the trailing edge causes unsteady flow phenomena that prevent the retention of type I interaction. The small boundary-layer separation seen in the pictures with type I interaction also increases the effective body surface deflection angle and contributes to the early transition to type II interaction.

The schlieren photographs of figure 14 give a better idea of the effect of the longitudinal position of the body upon the interference shock formation. The photographs for type I shock interaction data were selected from those made while the body surface deflection angle was increasing, and the photographs for the type II shock interaction were selected from those made while the body surface deflection angle was decreasing. All the schlieren pictures are for body and shock generator surface deflection angles of 30° and 16°, respectively. These angles are such that a shock interaction of either type I or type II is possible over a range of angles when the body is located at $\chi < 4.45$ cm. For values of χ somewhere between 3.81 and 6.35 cm, the change from type I to type II occurs over a narrow range of values of δ_D because of body interference. At $\chi \geqq 6.35$ cm, the interaction cannot be classified as type II because the bow shock of the body is detached.

In order to compare the extent of the region where either type I or type II shock interaction may occur, the theoretical extent of this region is determined graphically for all three shock generator angles in figure 15. A comparison of the range of type I and type II shock interaction as shown exper-

imentally in figures 10 and 11 with the range shown theoretically in figure 6 is illustrated in figure 16. The theoretical curve is identical to the curve of figure 6. The data represented as circular symbols are for greatest persistence of type I interaction and latest recurrence of type I interaction, and the data represented as square symbols are for the greatest persistence of type II interaction and the latest recurrence of type II interaction. The experimental range of shock pattern duplicity is not so extensive as the theoretical one. As mentioned previously, a type I interference shock pattern becomes more unstable and more likely to change to type II interaction as the border which precludes type I interaction is approached. Having been established, type II interaction remains stable and yields evenly to a reduction in body surface deflection angle until the strong shock segment of the type II interaction is nearly imperceptible before it finally disappears.

The effect seen previously in the schlieren photographs when the trailing shock from the shock intersection struck the trailing edge of the body is illustrated again in figure 17. The region of overlap where either a type I or type II shock interaction pattern may occur remains nearly constant as χ increases until it collapses rather sharply between χ = 3.81 and 5.08 cm. Once the proximity of the body takes effect, the type of interaction is no longer predictable by theoretical analysis. Edney (ref. 2) discusses the effects of the proximity of various bodies, including the wedge, on the shock intersection patterns and the solution by shock polars. The reduced angles at which type II interaction may occur at larger values of χ suggest that the higher effective surface deflection angles brought about by boundary-layer separation also contribute to the earlier transition to type II interaction.

CONCLUDING REMARKS

The shock strengths for which either Edney type I or type II shock interference patterns can occur when two oblique shocks of opposite families intersect have been determined graphically at Mach 10 by using logarithmic-shock-polar diagrams. The theoretical region of overlap for the two types of interaction was investigated by observing in the schlieren system of the Langley 15-inch hypersonic flow apparatus the intersection of oblique shocks generated by two sharp 10° wedges as the edge angles of attack and their relative positions were altered.

The results from this investigation show a range of shock strengths for which either of the two interference patterns (Edney type I or type II) can exist. The range of conditions is smaller in extent than theoretically expected, and the two types of interactions are not equally likely throughout the region. The type of pattern is also affected by the relative position of the shock interaction to the primary body.

Langley Research Center
National Aeronautics and Space Administration
Hampton, VA 23665
August 14, 1979

REFERENCES

1. Courant, R.; and Friedrichs, K. O.: Supersonic Flow and Shock Waves. Interscience Publ., Inc., 1948.

2. Edney, Barry: Anomalous Heat Transfer and Pressure Distributions on Blunt Bodies at Hypersonic Speeds in the Presence of an Impinging Shock. FFA Rep. 115, Aeronaut. Res. Inst. of Sweden, 1968.

3. Crawford, Davis, H.: A Graphical Method for the Investigation of Shock Interference Phenomena. AIAA J., vol. 11, no. 11, Nov. 1973, pp. 1590-1592.

4. Edney, B. E.; Bramlette, T. T.; Ives, J.; Hains, F. D.; and Keyes, J. W.: Theoretical and Experimental Studies of Shock Interference Heating. Rep. No. 9500-920-195 (Contract NAS1-9606), Bell Aerospace Co., Oct. 1970.

5. Keyes, J. Wayne; and Hains, Frank D.: Analytical and Experimental Studies of Shock Interference Heating in Hypersonic Flows. NASA TN D-7139, 1973.

6. Keyes, J. Wayne: Off-Center-Line Shock-Interference Heating Patterns on Basic Shapes in Hypersonic Flow. NASA TM X-2866, 1973.

7. Barnette, Daniel W.: An Experimental Investigation of Supersonic Flow Past a Wedge-Cylinder Configuration. NASA CR-147741, 1976.

8. Kaufman, Louis G., II; Korkegi, Robert H.; and Morton, Leo C.: Shock Impingement Caused by Boundary Layer Separation Ahead of Blunt Fins. ARL-72-0118, U.S. Air Force, Aug. 1972.

9. Shapiro, Ascher H.: The Dynamics and Thermodynamics of Compressible Fluid Flow. Vol. II. Ronald Press Co., c.1954.

10. Ferri, Antonio: Elements of Aerodynamics of Supersonic Flows. Macmillan Co., 1949.

11. Morris, Dana J.; and Keyes, J. Wayne: Computer Programs for Predicting Supersonic and Hypersonic Interference Flow Fields and Heating. NASA TM X-2725, 1973.

12. Putnam, Lawrence E.; and Brooks, Cuyler W., Jr.: Static Longitudinal Aerodynamic Characteristics at a Mach Number of 10.03 of Low-Aspect-Ratio Wing-Body Configurations Suitable for Reentry. NASA TM X-733, 1962.

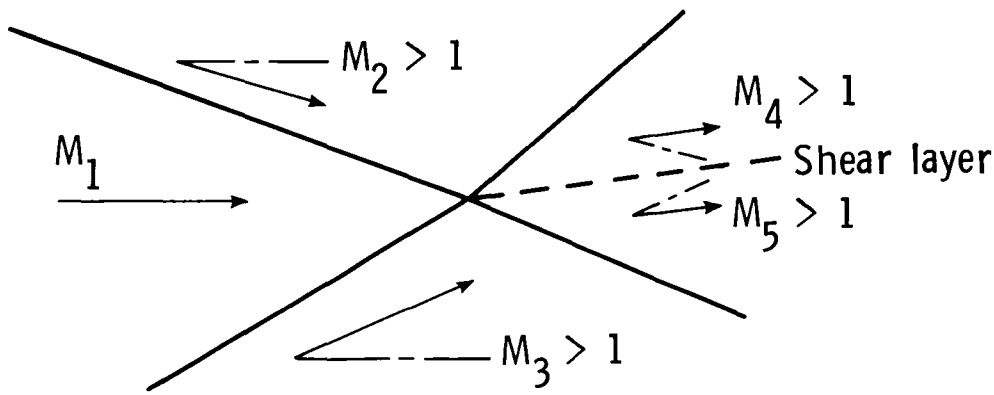

(a) Two weak shocks of opposite families.

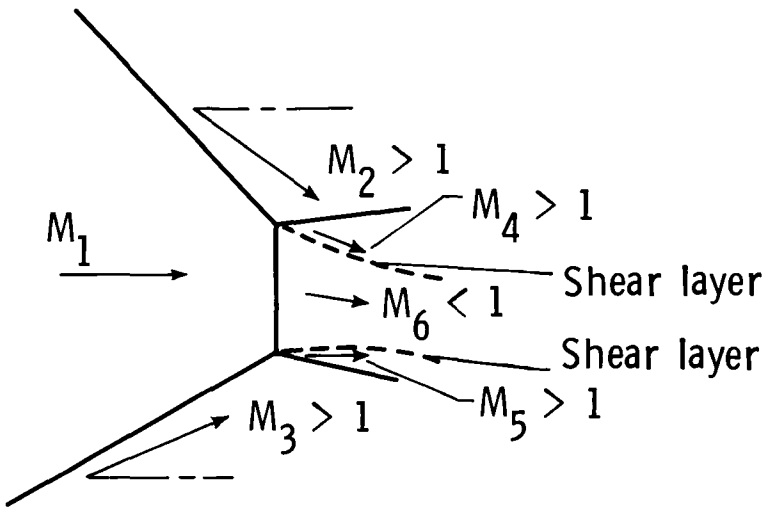

(b) Two weak shocks of opposite families when Mach reflection is necessary for equilibrium pressure.

Figure 1.- Examples of shock interaction at a point of $M_1 = 10$.

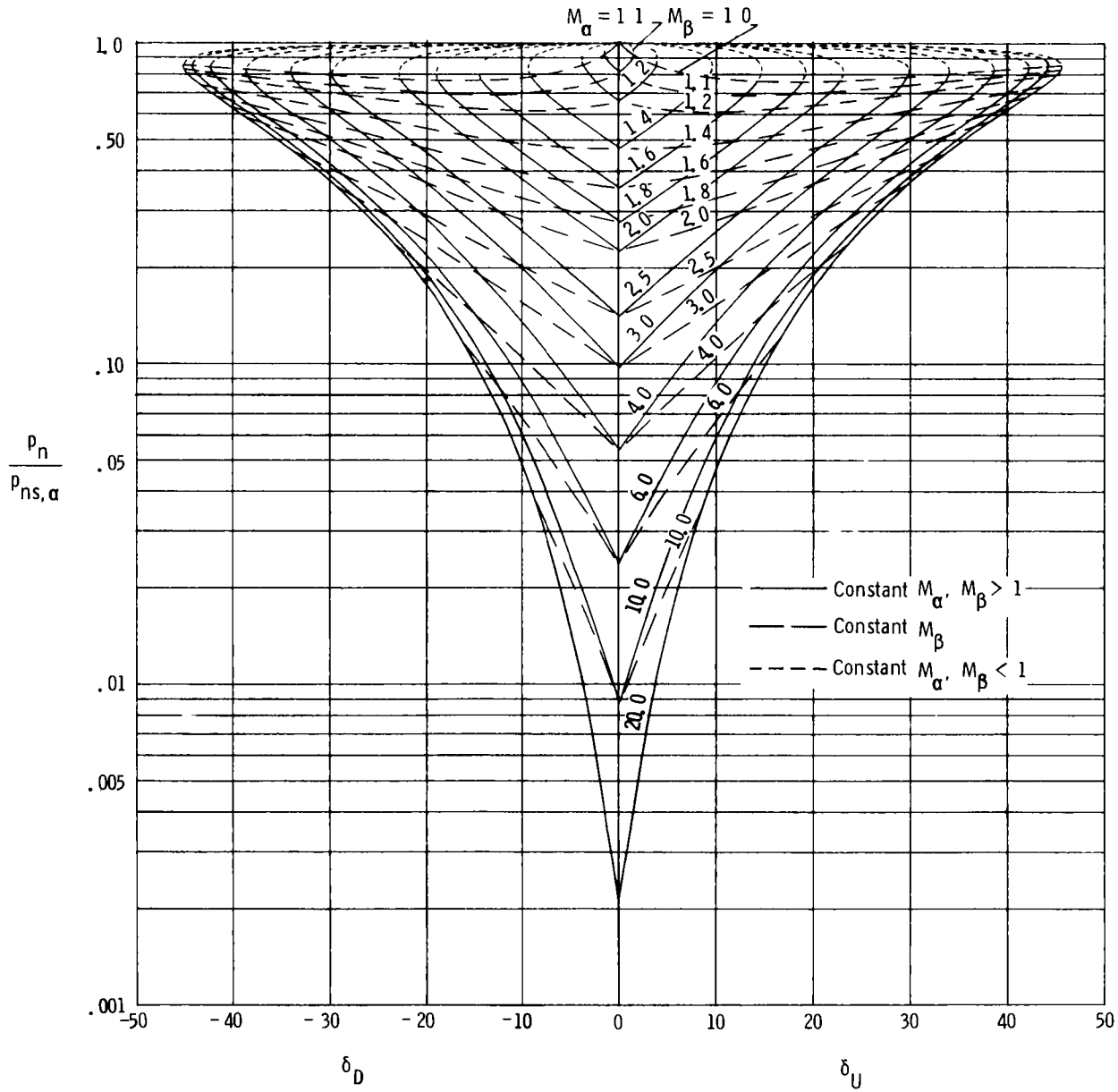

Figure 2.- Logarithmic-shock-polar family.

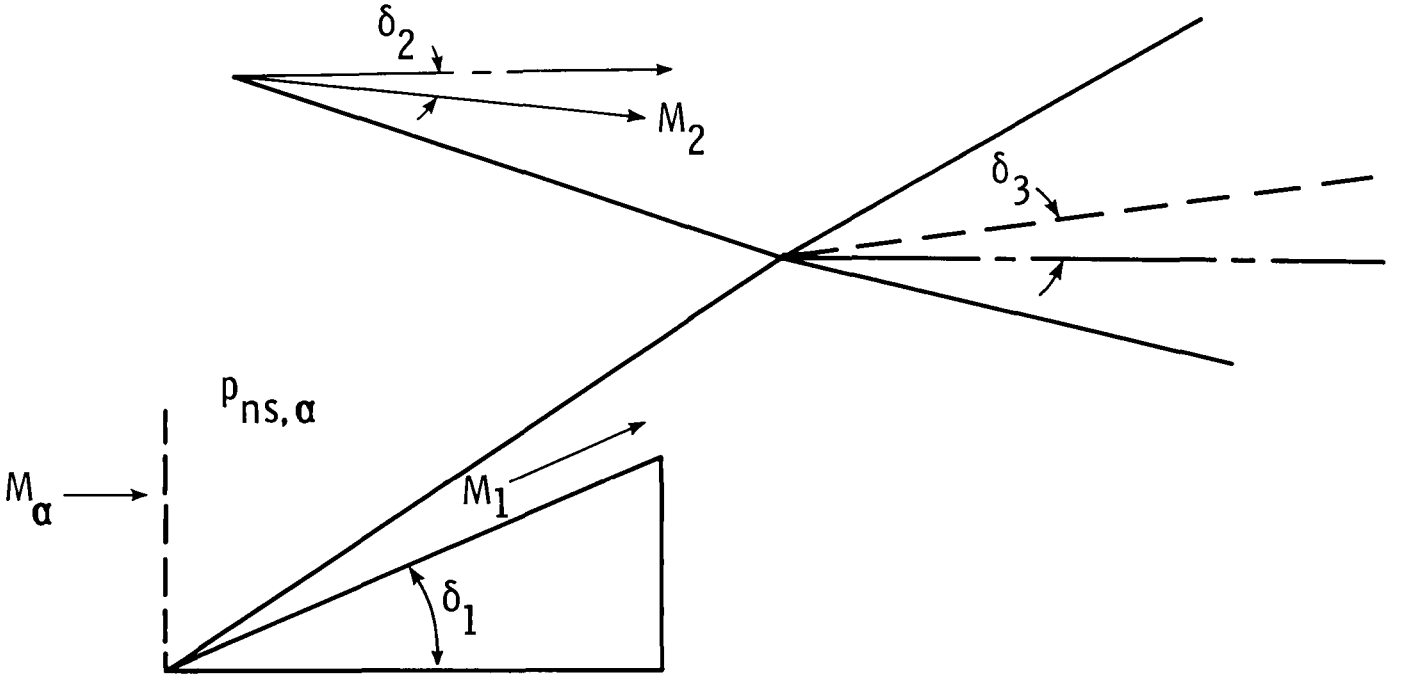

(a) Type of interaction calculated.

Figure 3.- Use of logarithmic-shock-polar diagram to calculate type I shock interaction.

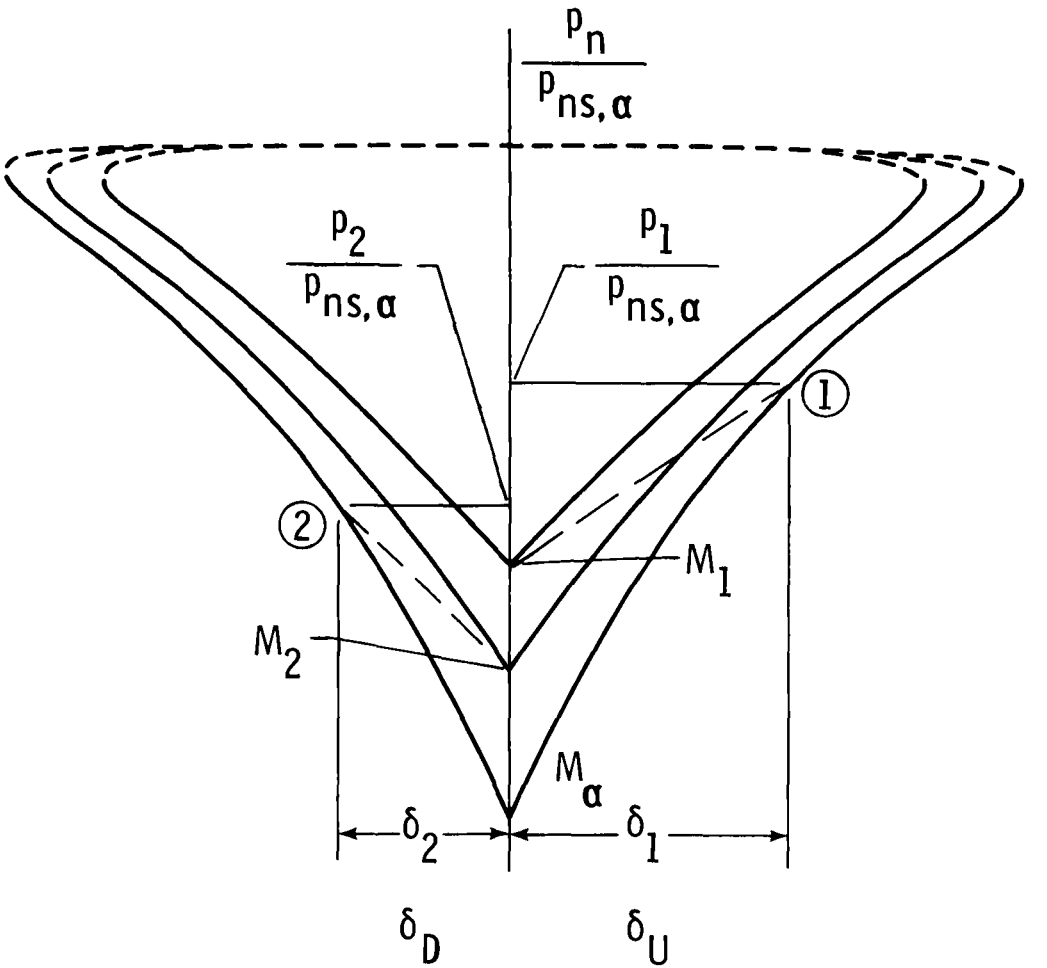

(b) Parts of logarithmic-shock-polar diagram used.

Figure 3.- Continued.

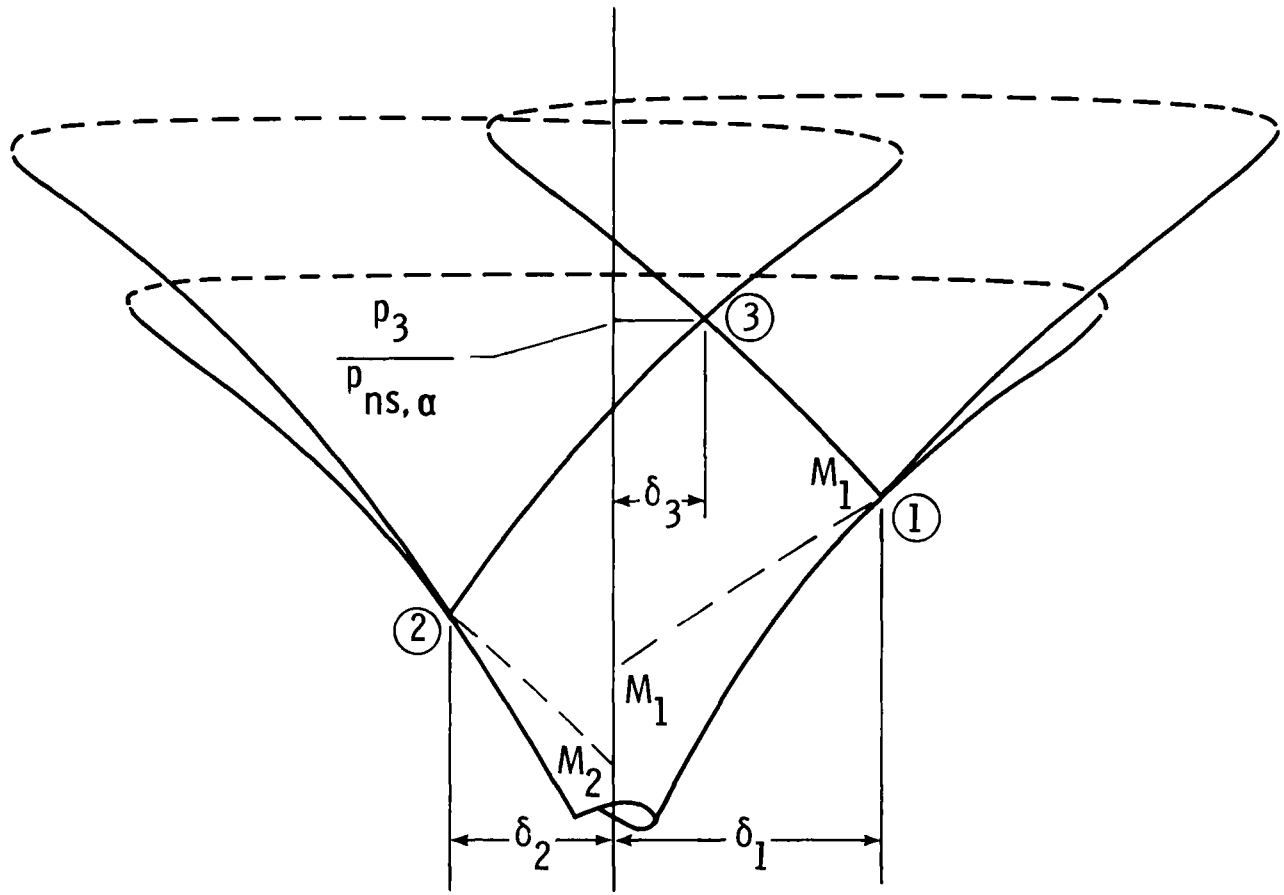

(c) Illustration of values of $p_3/p_{ns,\alpha}$ and δ_3 obtained.

Figure 3.- Concluded.

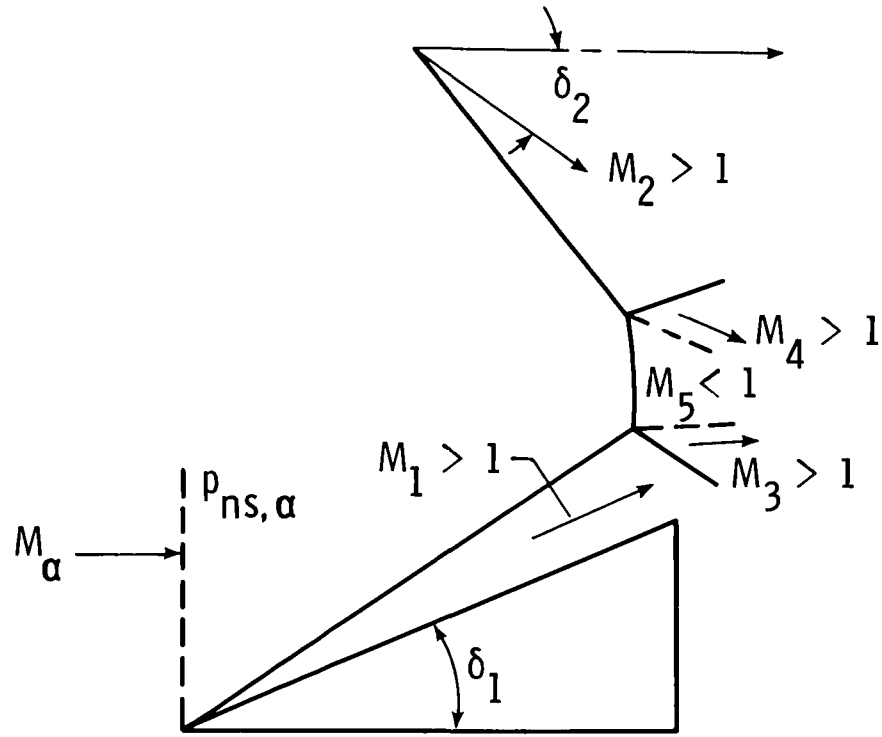

(a) Type of interaction calculated.

Figure 4.- Use of logarithmic-shock-polar diagram to calculate type II shock interaction.

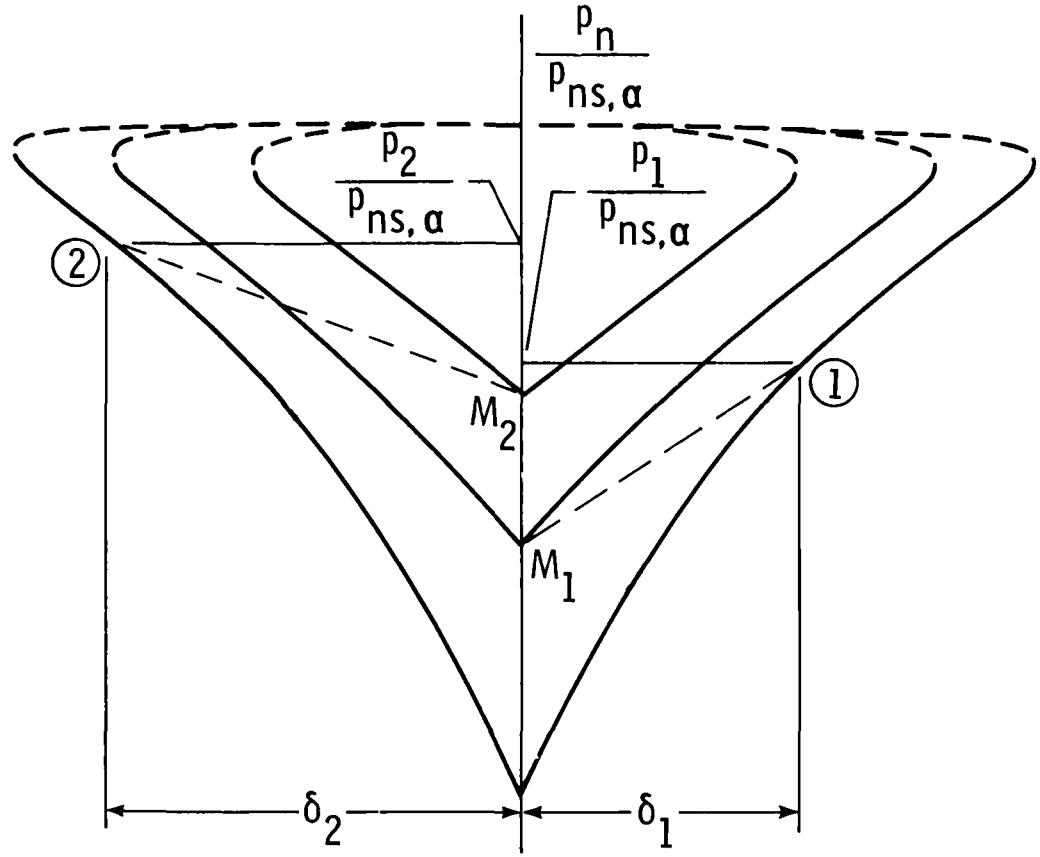

(b) Parts of logarithmic-shock-polar diagram used.

Figure 4.- Continued.

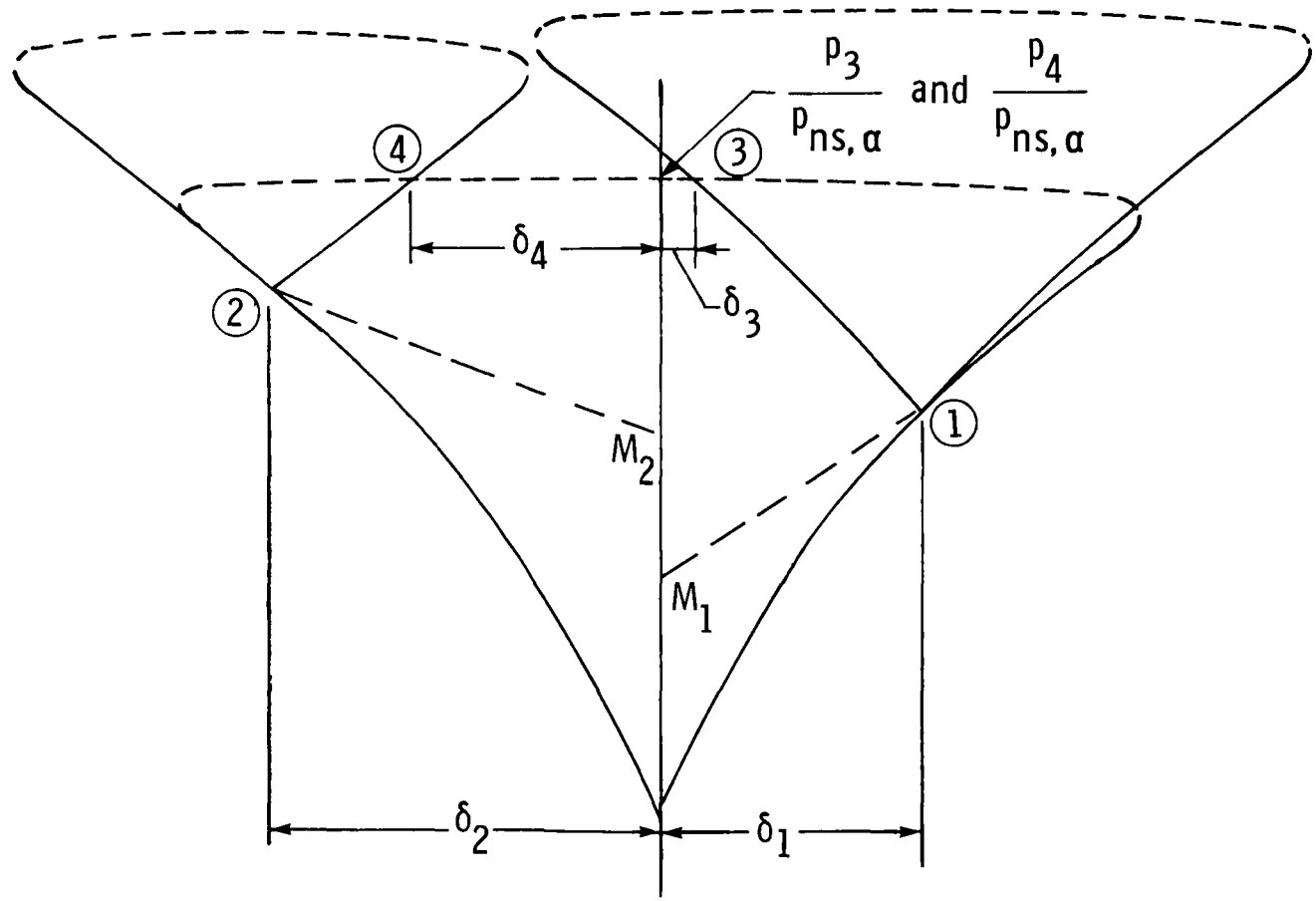

(c) Illustration of values of $p_3/p_{ns,\alpha}$, $p_4/p_{ns,\alpha}$, δ_3, and δ_4 obtained.

Figure 4.- Concluded.

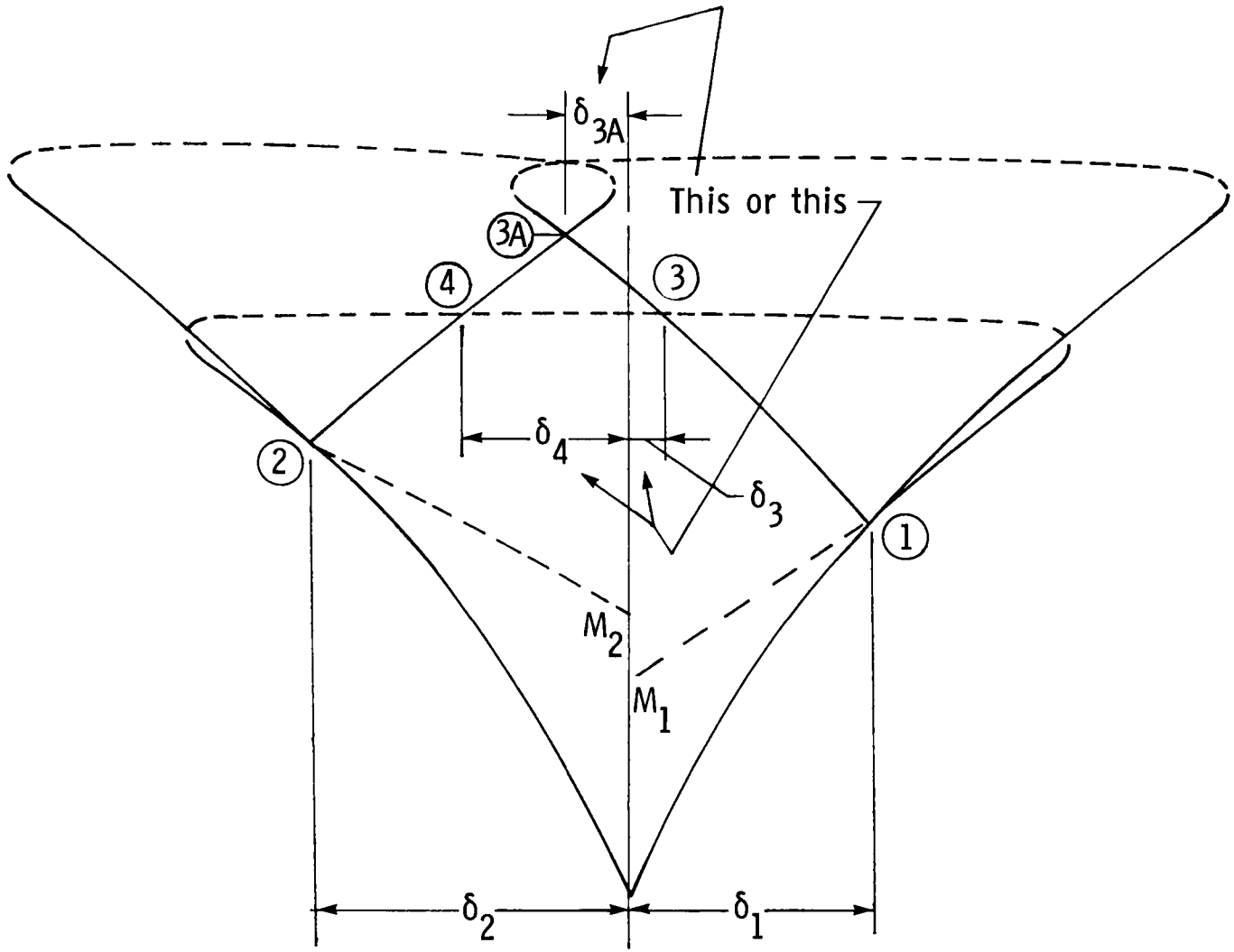

Figure 5.- Use of logarithmic-shock-polar diagram where either type I or type II shock interference is possible.

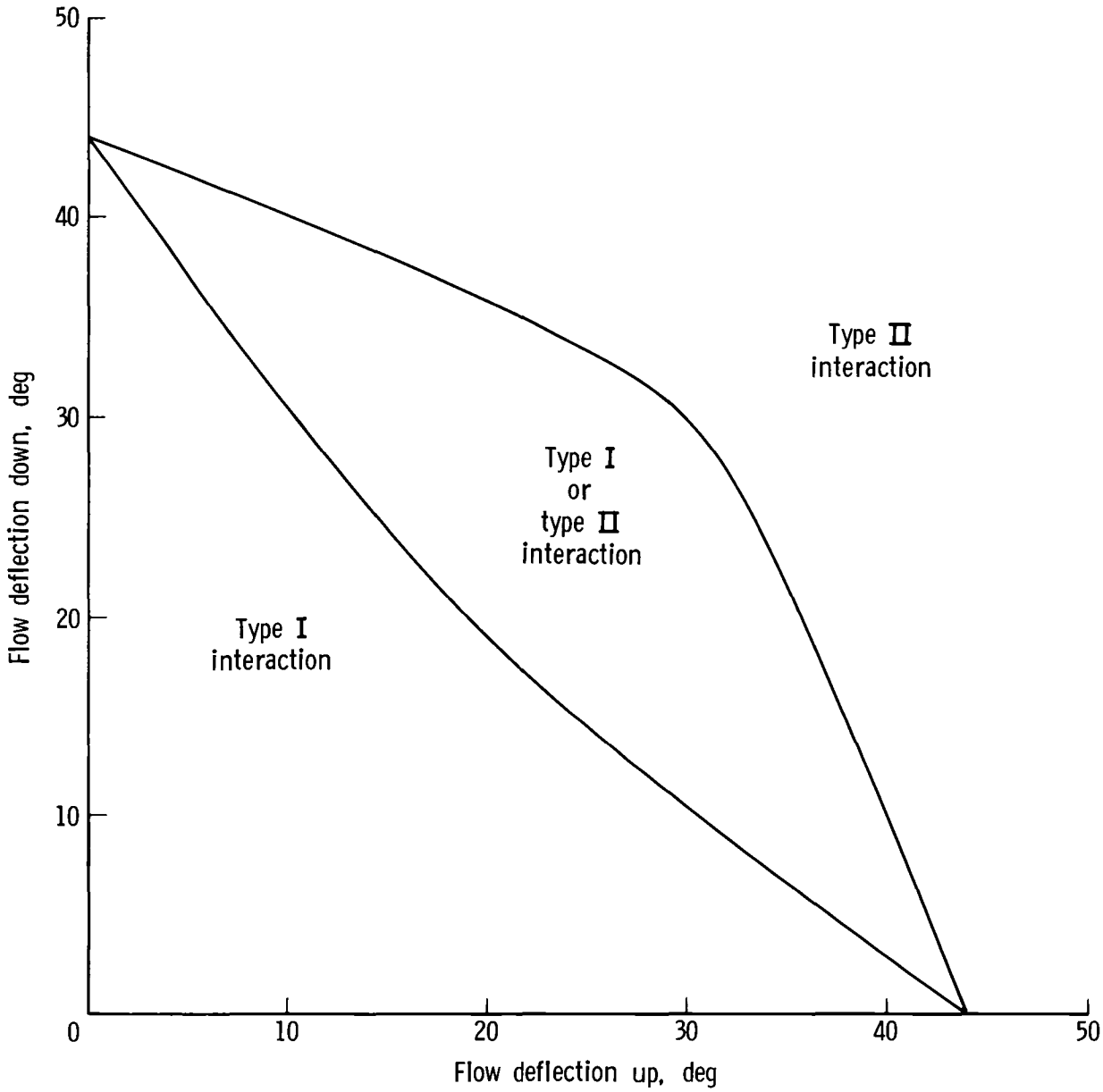

Figure 6.- Theoretically determined envelope for maximum possible overlap of interference shock generator and body surface deflection angles where either type I or type II interaction may occur at Mach 10.

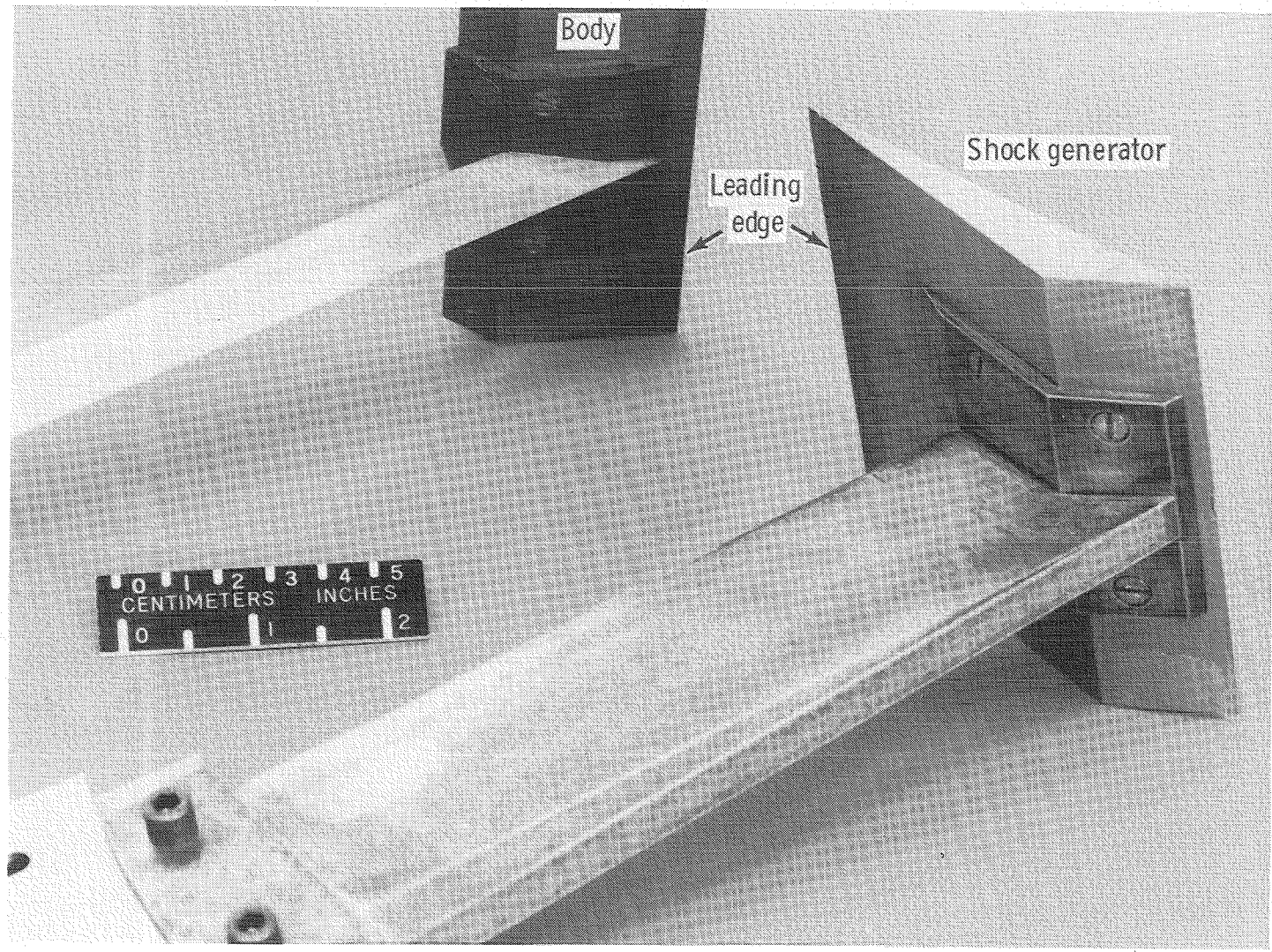

L-79-1129.1

(a) Wedges.

Figure 7.- Detailed photographs of models.

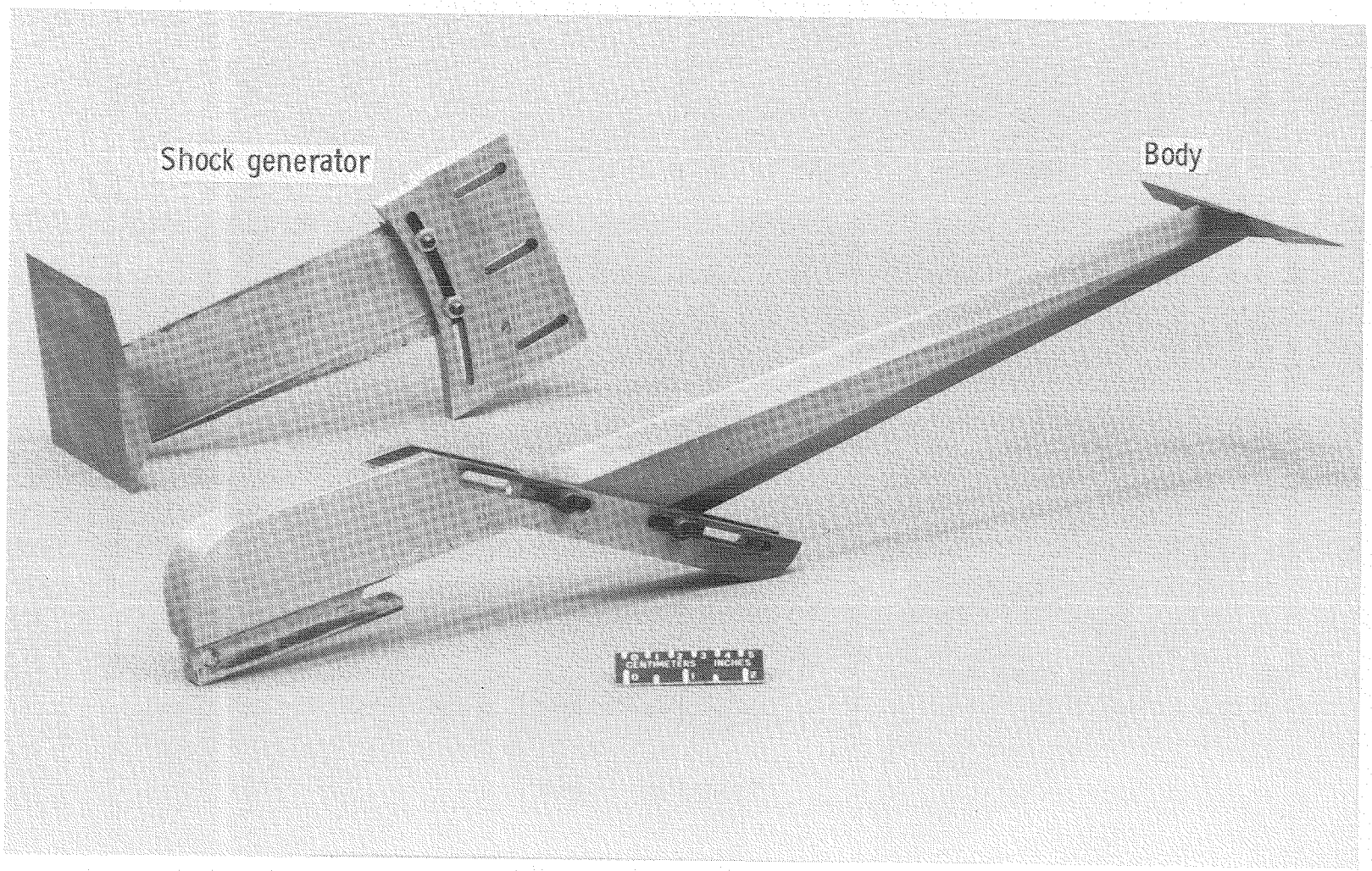

L-79-1130.1

(b) Wedges and mounts.

Figure 7.- Concluded.

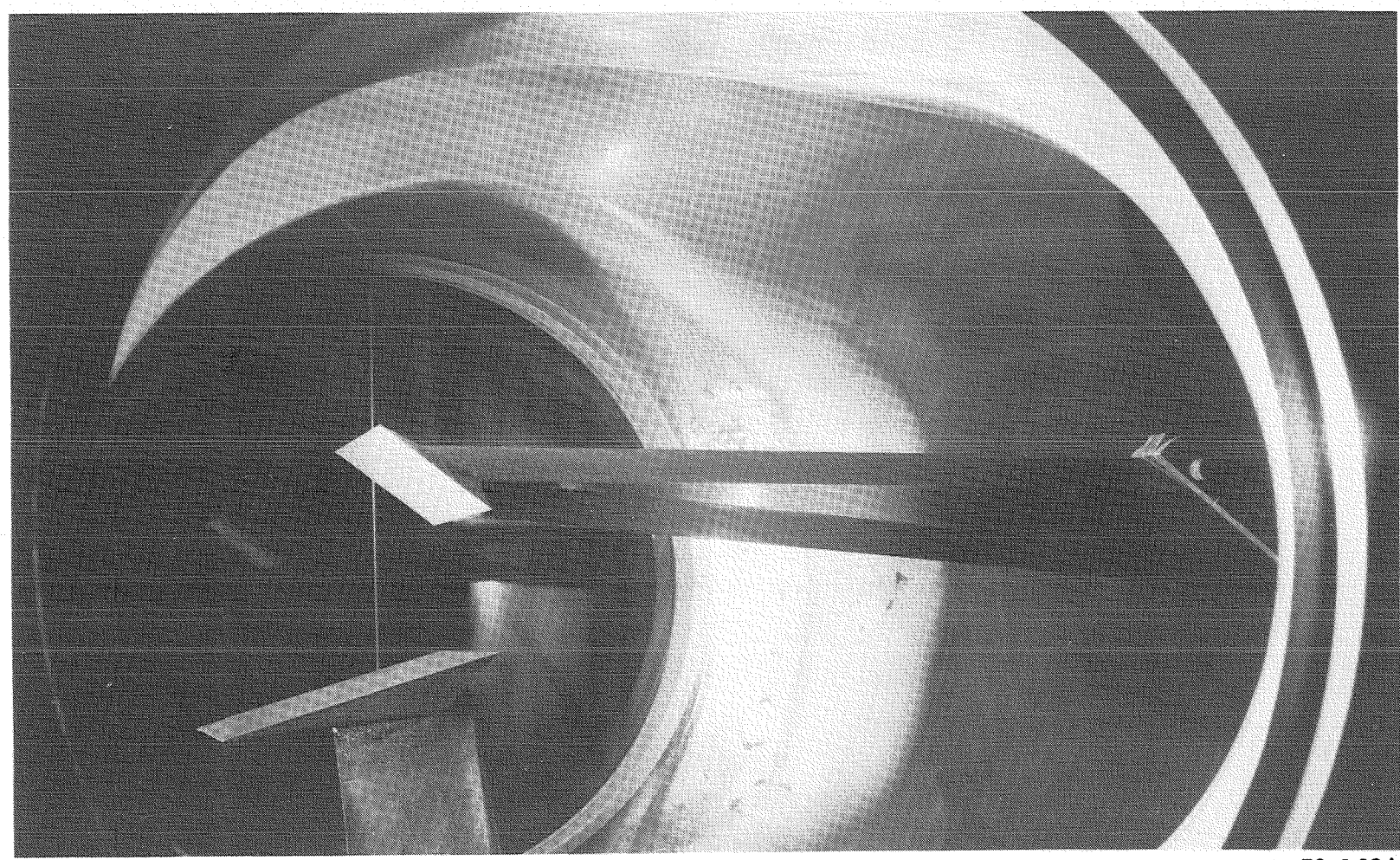

L-78-1934

Figure 8.- Photograph of models in tunnel.

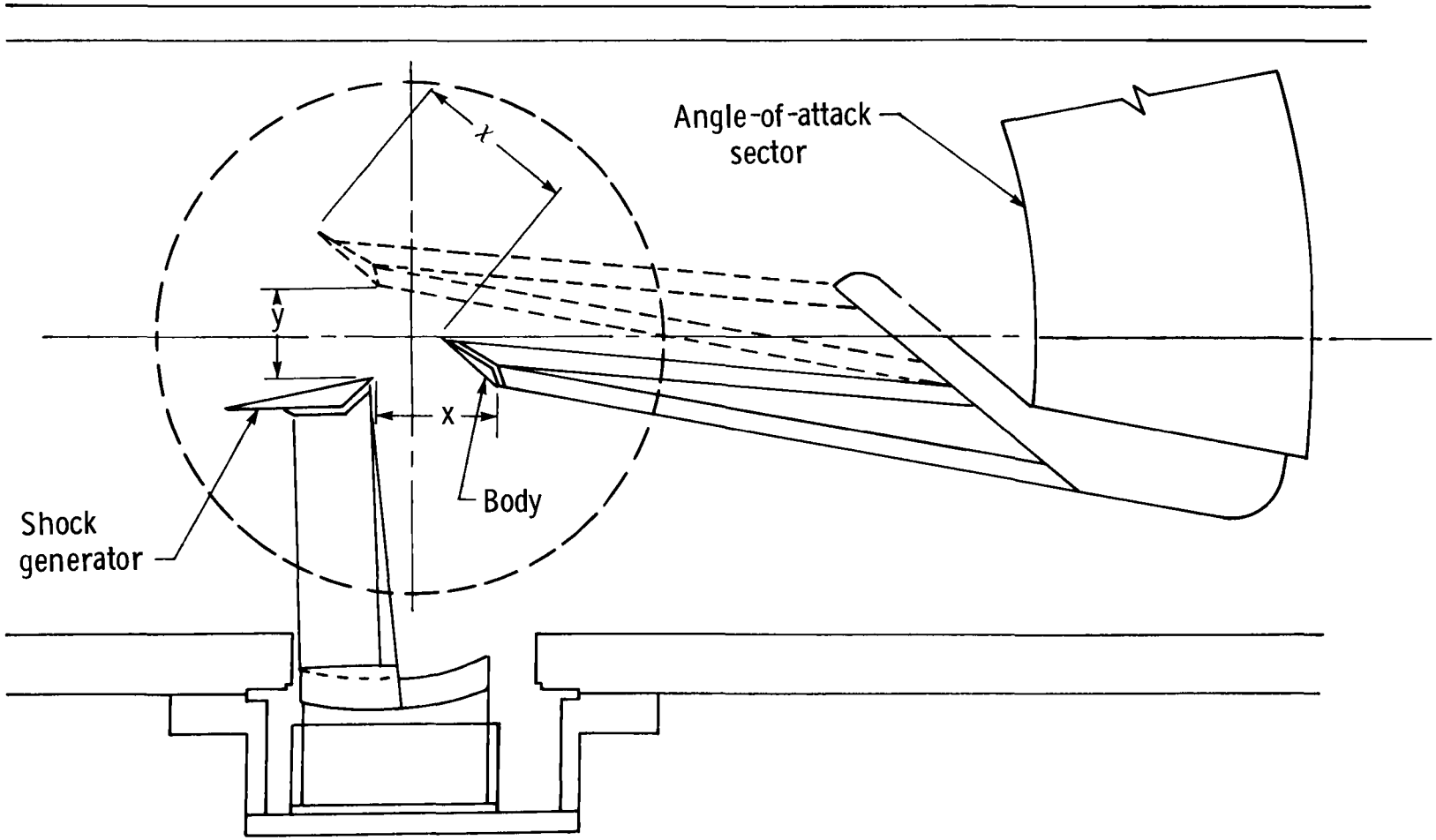

Figure 9.- Diagram of models mounted for test in tunnel.

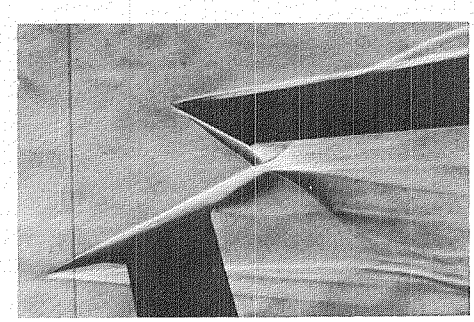

(a) $\delta_D = 28^o$.

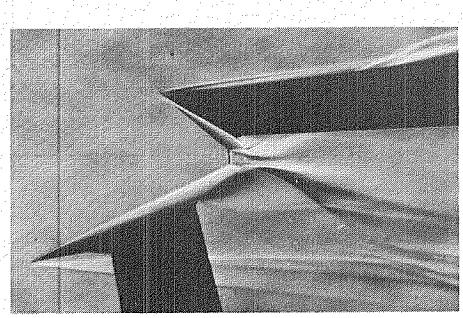

(b) $\delta_D = 29^o$.

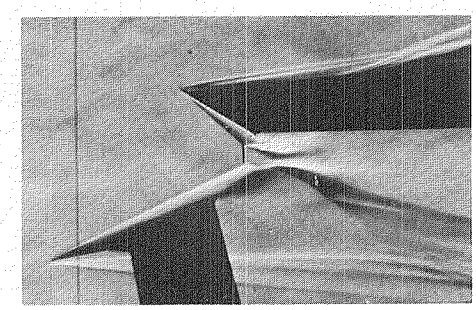

(c) $\delta_D = 31^o$.

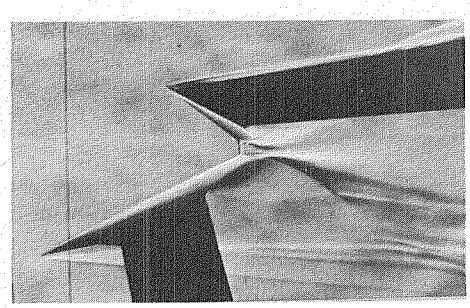

(d) $\delta_D = 28^o$.

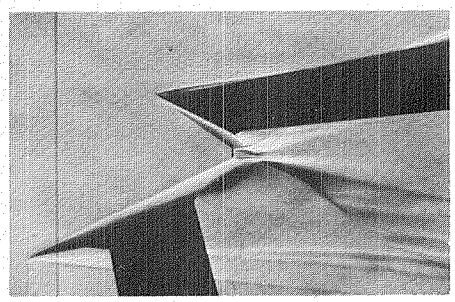

(e) $\delta_D = 26^o$.

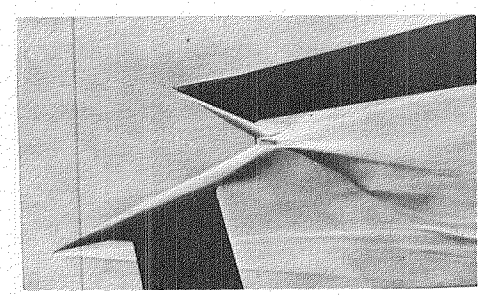

(f) $\delta_D = 24^o$.

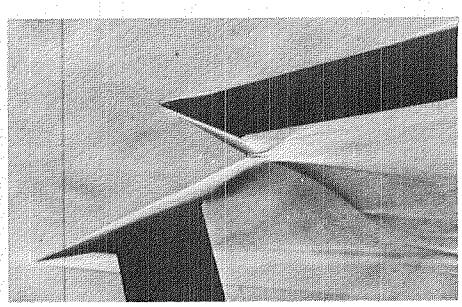

(g) $\delta_D = 22^o$.

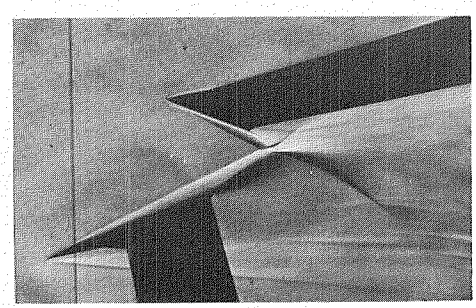

(h) $\delta_D = 21^o$.

L-79-281

Figure 10.- Example of range of surface deflection angles where either type I or type II interaction may exist. $\delta_U = 20^o$; $\chi = 2.54$ cm; $x = 2.00$ cm; $y = 3.45$ cm.

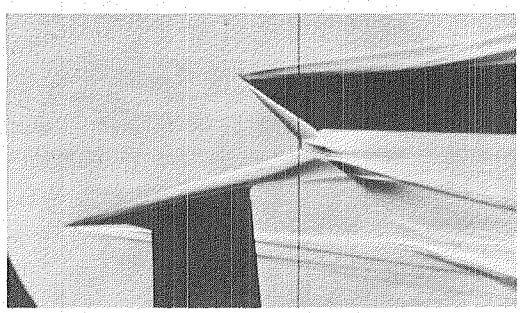

(a) $\delta_D = 34^o$.

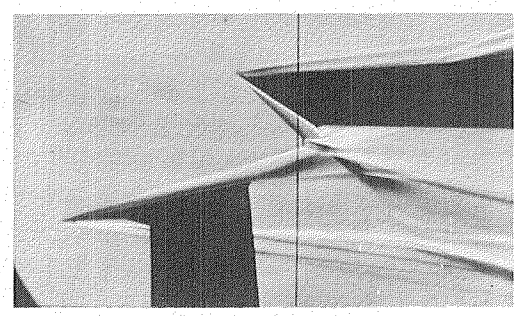

(b) $\delta_D = 33^o$.

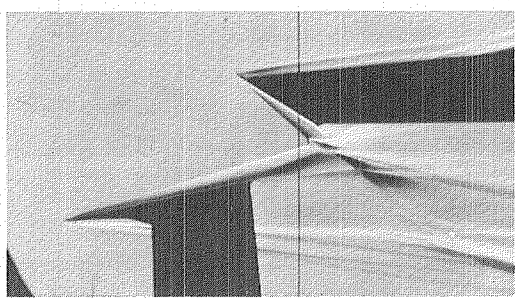

(c) $\delta_D = 32^o$.

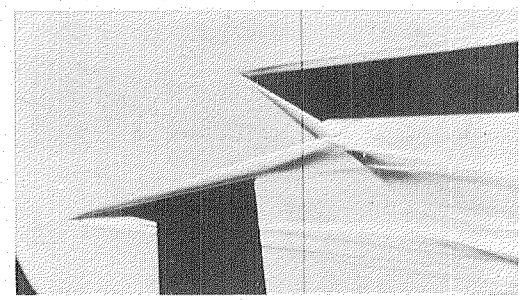

(d) $\delta_D = 31^o$.

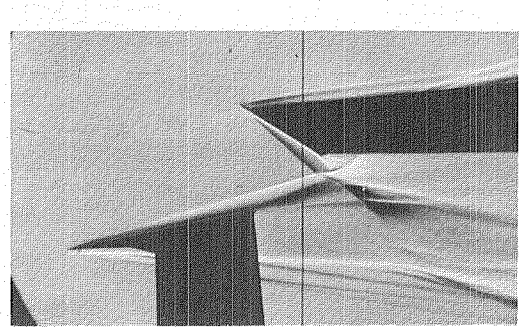

(e) $\delta_D = 32^o$.

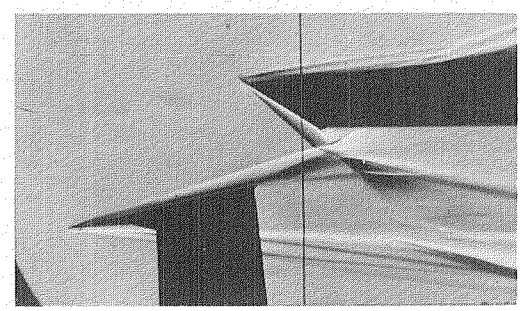

(f) $\delta_D = 33^o$.

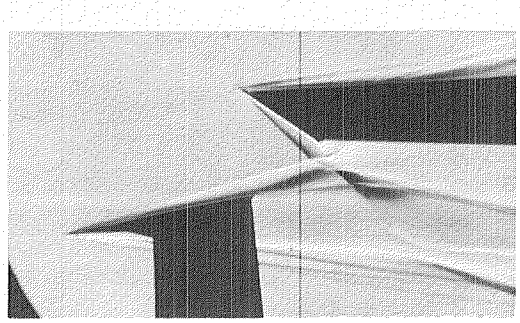

(g) $\delta_D = 34^o$.

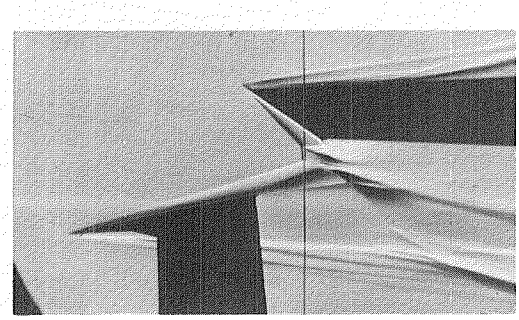

(h) $\delta_D = 35^o$.

L-79-282

Figure 11.- Example of shock interaction change caused by surface deflection angle-of-attack change. $\delta_U = 12^o$; $\chi = 3.81$ cm; $x = 3.19$ cm; $y = 2.74$ cm.

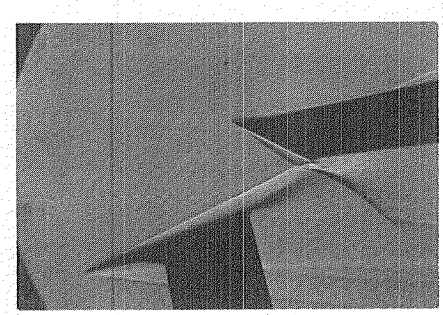

(a) $\delta_D = 26^o$.

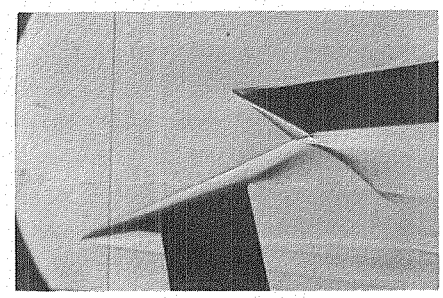

(b) $\delta_D = 27^o$.

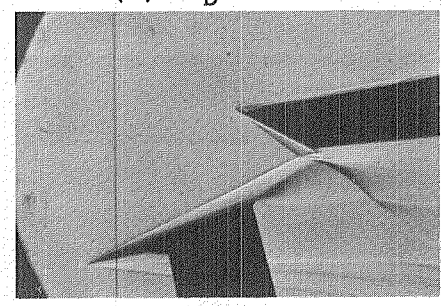

(c) $\delta_D = 28^o$.

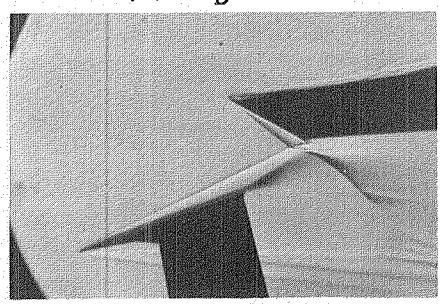

(d) $\delta_D = 29^o$.

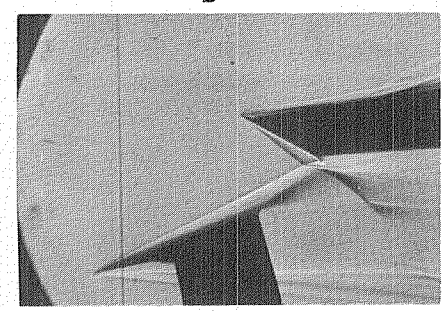

(e) $\delta_D = 30^o$.

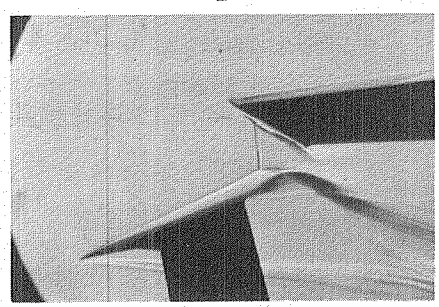

(f) $\delta_D = 31^o$.

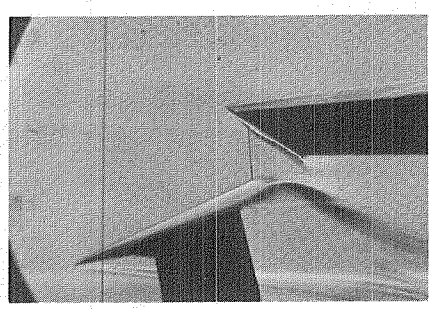

(g) $\delta_D = 32^o$.

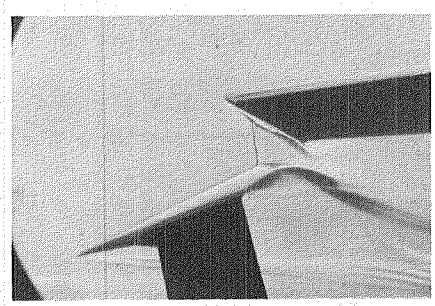

(h) $\delta_D = 30^o$.

L-79-283

Figure 12.- Example where large tendency exists for either type I or type II interaction to occur. $\delta_U = 20^o$; $\chi = 3.81$ cm; $x = 3.87$ cm; $y = 2.93$ cm.

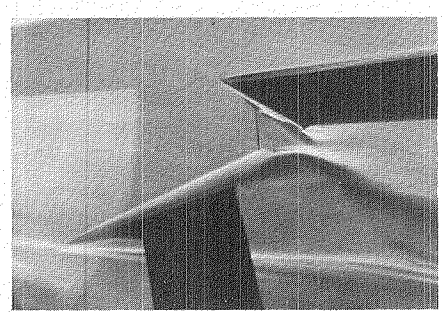

(i) $\delta_D = 29^o$.

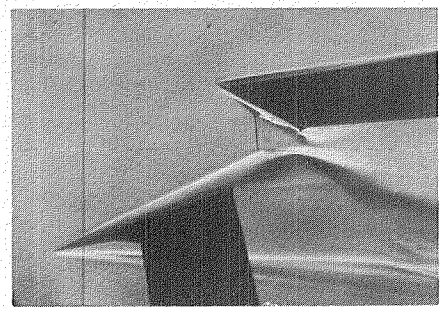

(j) $\delta_D = 28^o$.

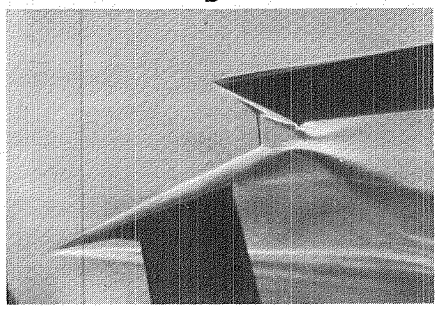

(k) $\delta_D = 27^o$.

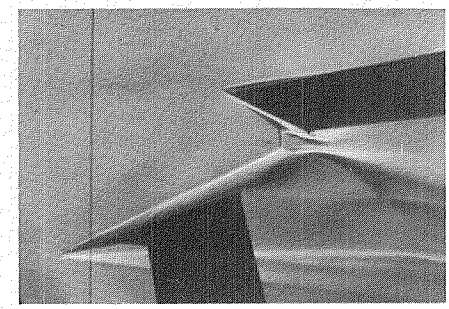

(l) $\delta_D = 26^o$.

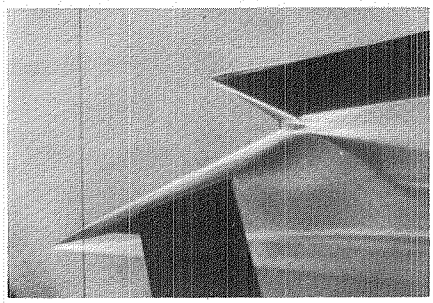

(m) $\delta_D = 25^o$.

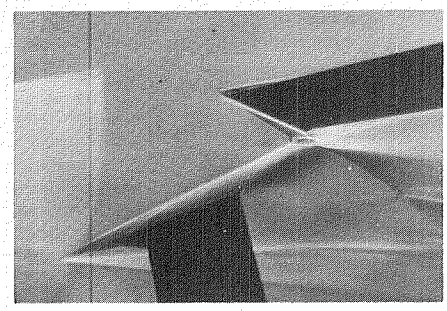

(n) $\delta_D = 24^o$.

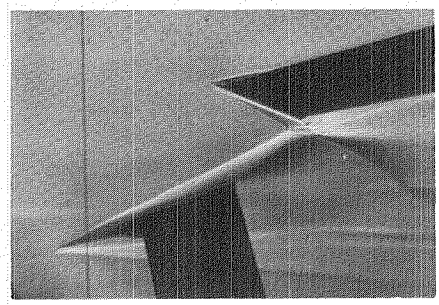

(o) $\delta_D = 23^o$.

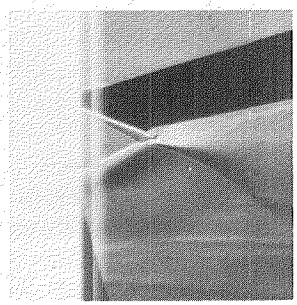

(p) $\delta_D = 22^o$.

L-79-284

Figure 12.- Concluded.

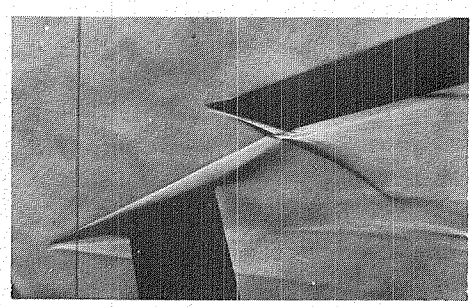

(a) $\delta_D = 17^o$.

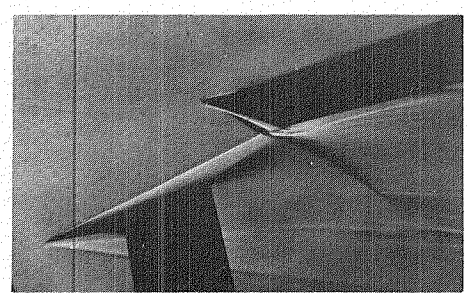

(b) $\delta_D = 18^o$.

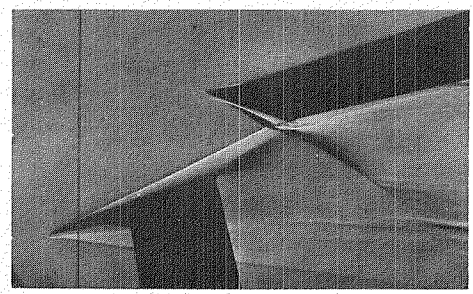

(c) $\delta_D = 19^o$.

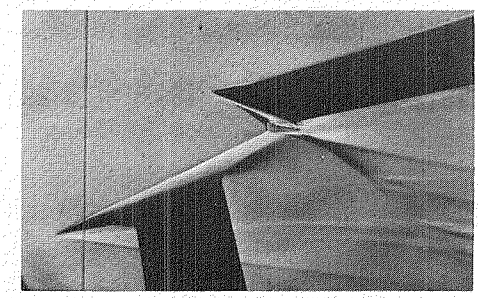

(d) $\delta_D = 20^o$.

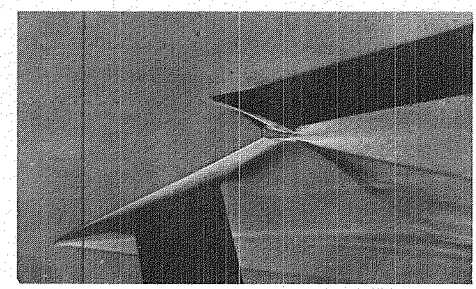

(e) $\delta_D = 21^o$.

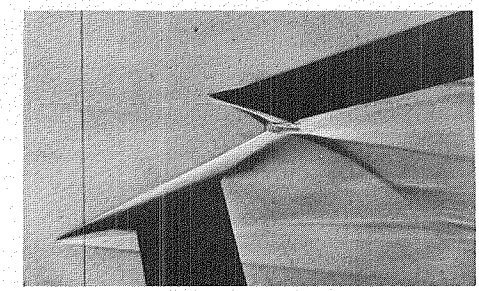

(f) $\delta_D = 19^o$.

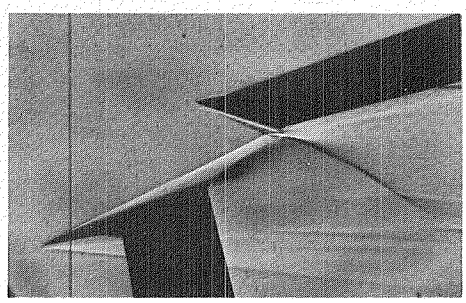

(g) $\delta_D = 18^o$.

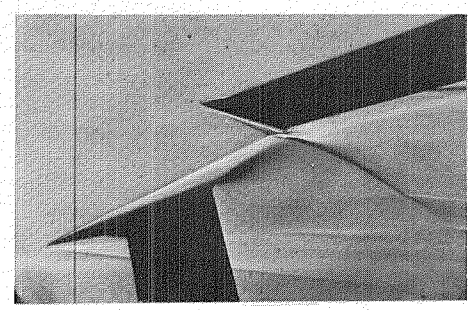

(h) $\delta_D = 17^o$.

L-79-285

Figure 13.- Example where small tendency exists for either type I or type II interaction to occur. $\delta_U = 20^o$; $\chi = 4.45$ cm; $x = 3.23$ cm; $y = 2.83$ cm.

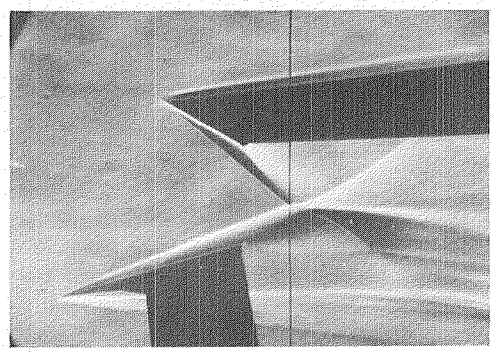

(a) Increasing δ_D; χ = 0 cm; x = 0 cm; y = 4.84 cm.

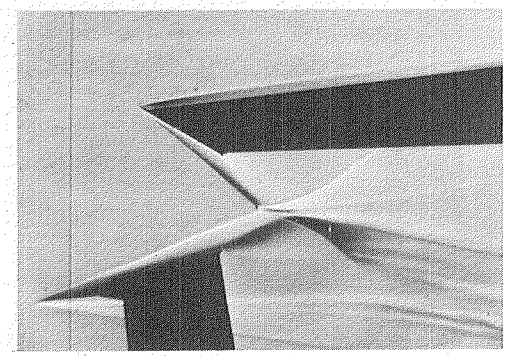

(b) Decreasing δ_D; χ = 0 cm; x = -0.16 cm; y = 4.80 cm.

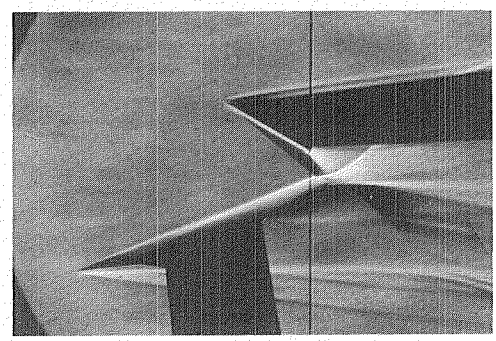

(c) Increasing δ_D; χ = 2.54 cm; x = 2.18 cm; y = 3.51 cm.

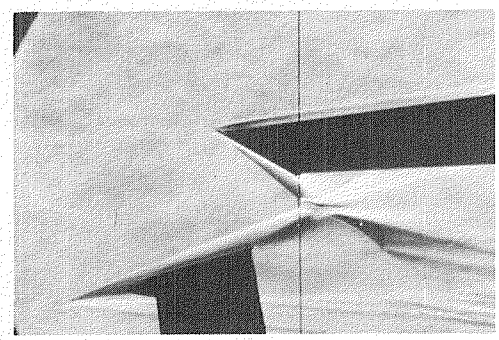

(d) Decreasing δ_D; χ = 2.54 cm; x = 2.18 cm; y = 3.51 cm.

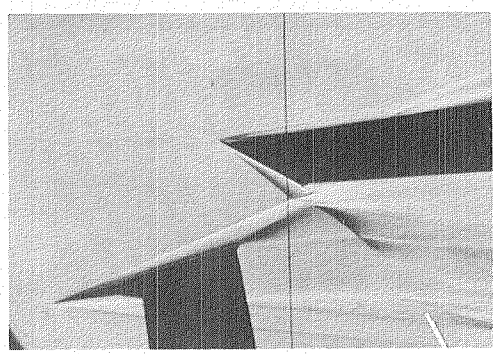

(e) Increasing δ_D; χ = 3.81 cm; x = 2.42 cm; y = 2.82 cm.

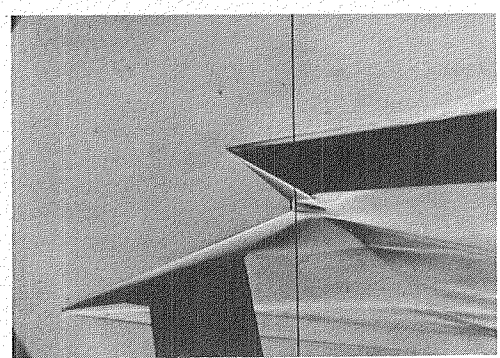

(f) Decreasing δ_D; χ = 3.81 cm; x = 2.42 cm; y = 2.82 cm.

L-79-286

Figure 14.- Shock interference patterns with body in several longitudinal positions along fixed plane relative to shock generator. $\delta_D = 30^\circ$; $\delta_U = 16^\circ$.

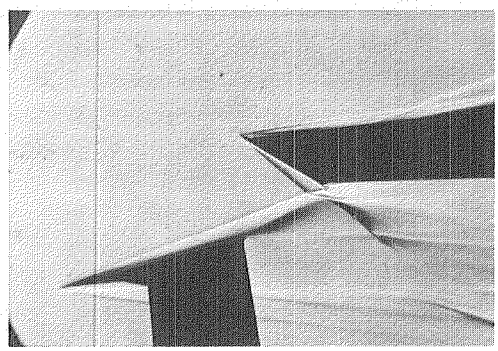

(g) Increasing δ_D; χ = 4.45 cm; x = 3.82 cm; y = 2.60 cm.

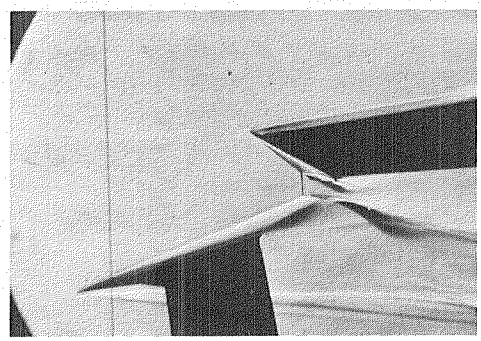

(h) Decreasing δ_D; χ = 4.45 cm; x = 3.82 cm; y = 2.60 cm.

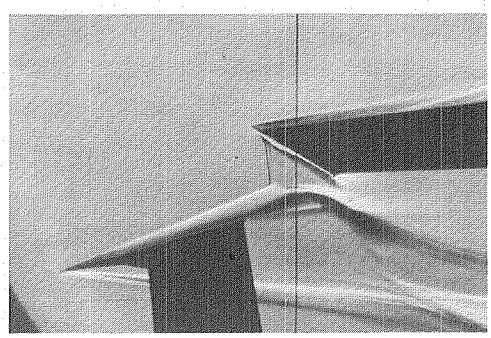

(i) Increasing δ_D; χ = 5.08 cm; x = 4.35 cm; y = 2.10 cm.

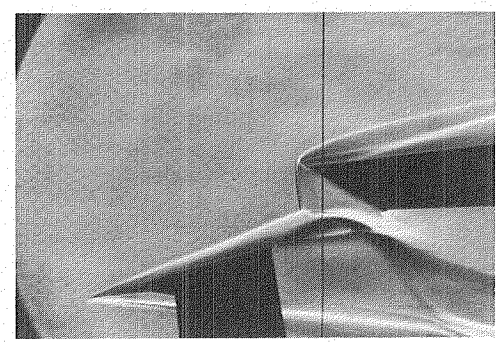

(j) Decreasing δ_D; χ = 6.35 cm; x = 5.48 cm; y = 1.69 cm.

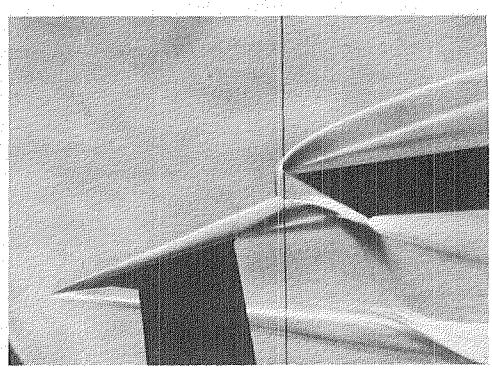

(k) Increasing δ_D; χ = 7.62 cm; x = 6.63 cm; y = 0.89 cm.

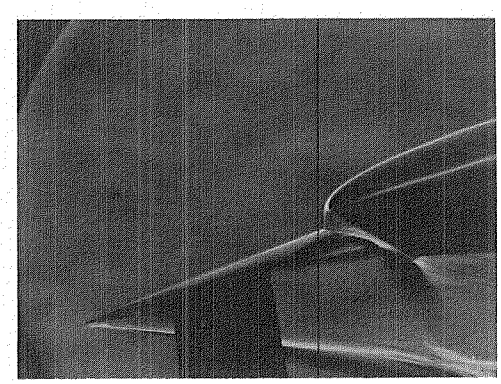

(l) Decreasing δ_D; χ = 8.26 cm; x = 7.18 cm; y = 0.40 cm.

L-79-287

Figure 14.- Concluded.

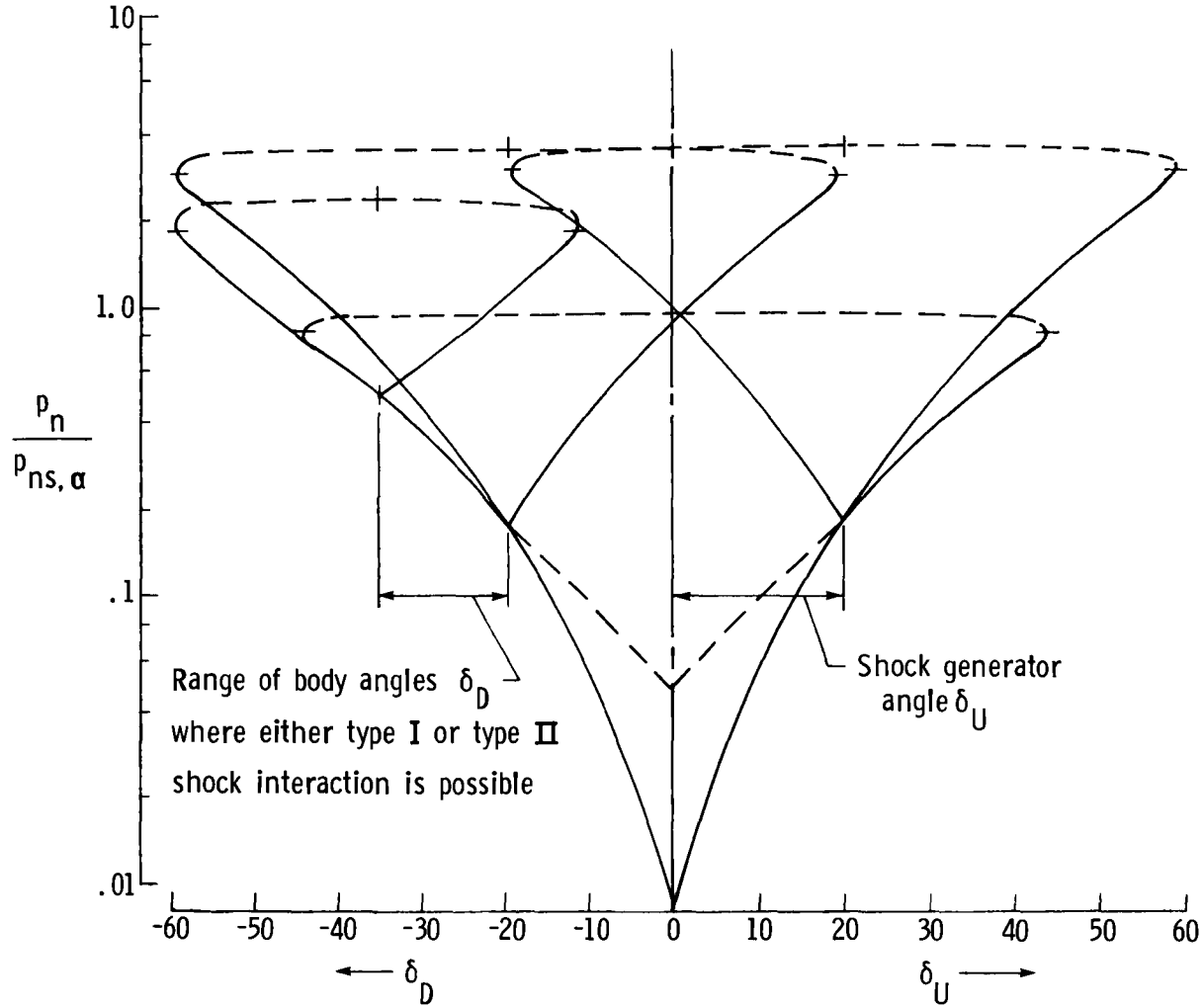

(a) $\delta_U = 20^\circ$.

Figure 15.- Graphical analysis of body angles where either type I or type II shock interaction is possible.

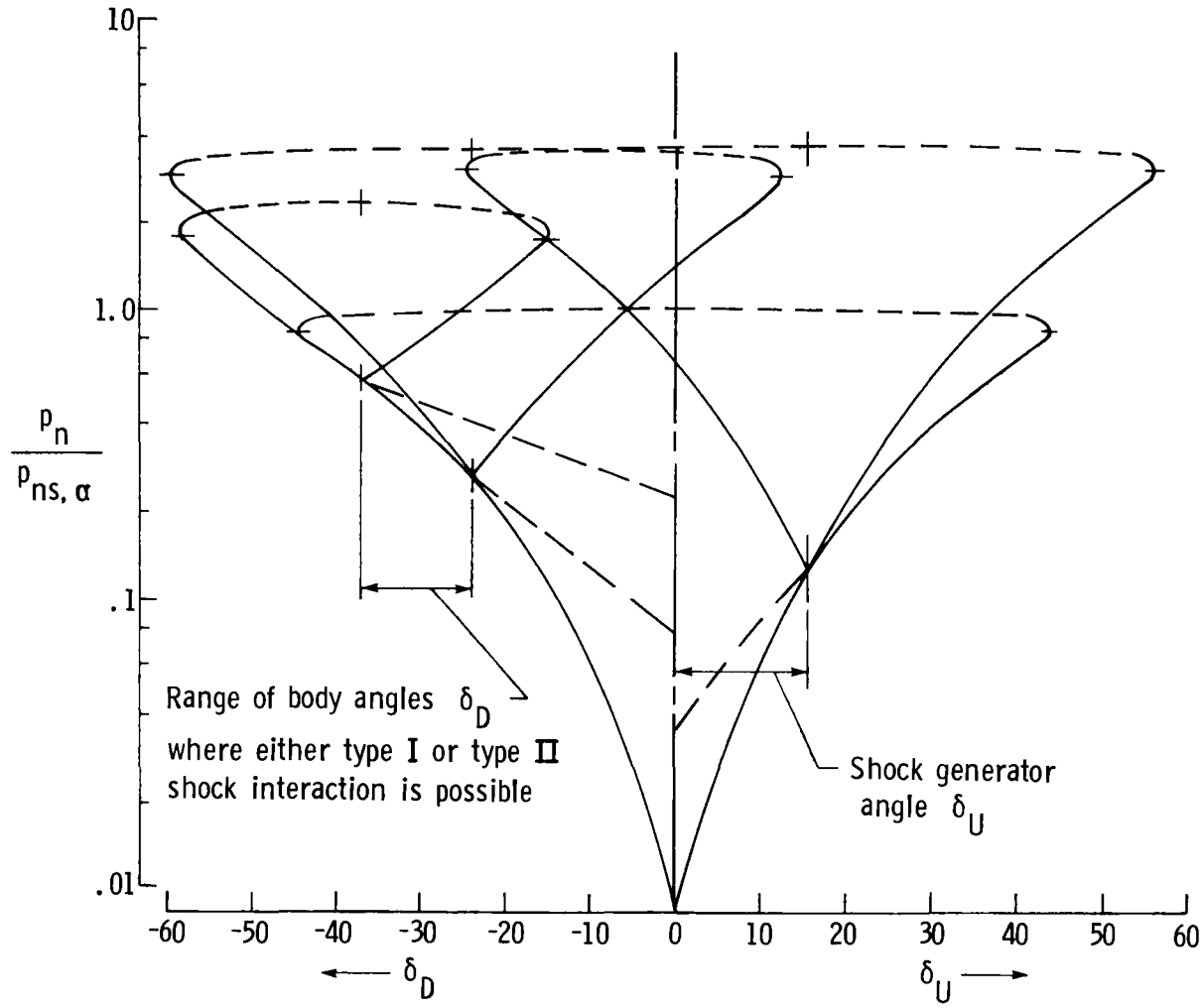

(b) $\delta_U = 16^\circ$.

Figure 15.- Continued.

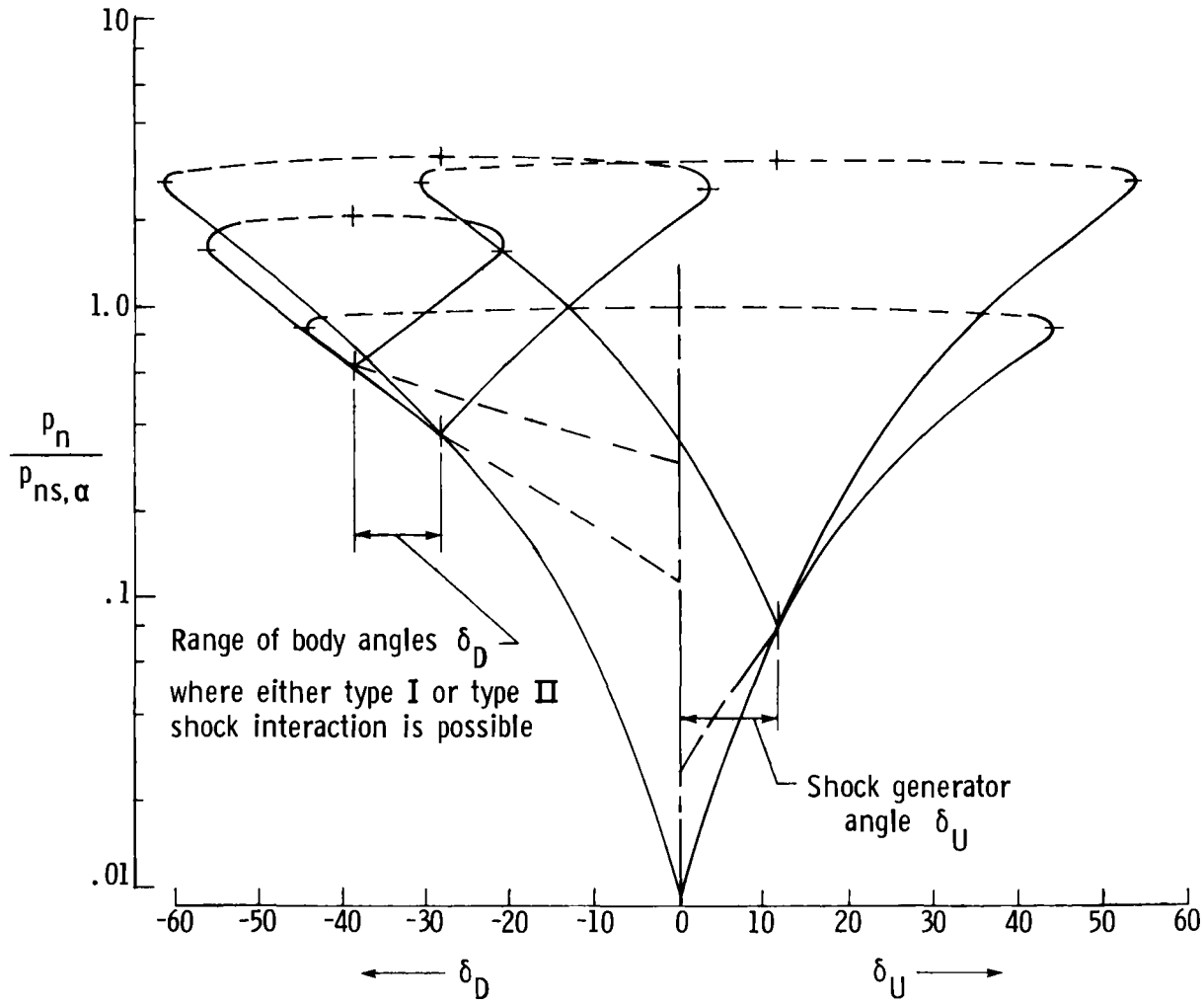

(c) $\delta_U = 12^o$.

Figure 15.- Concluded.

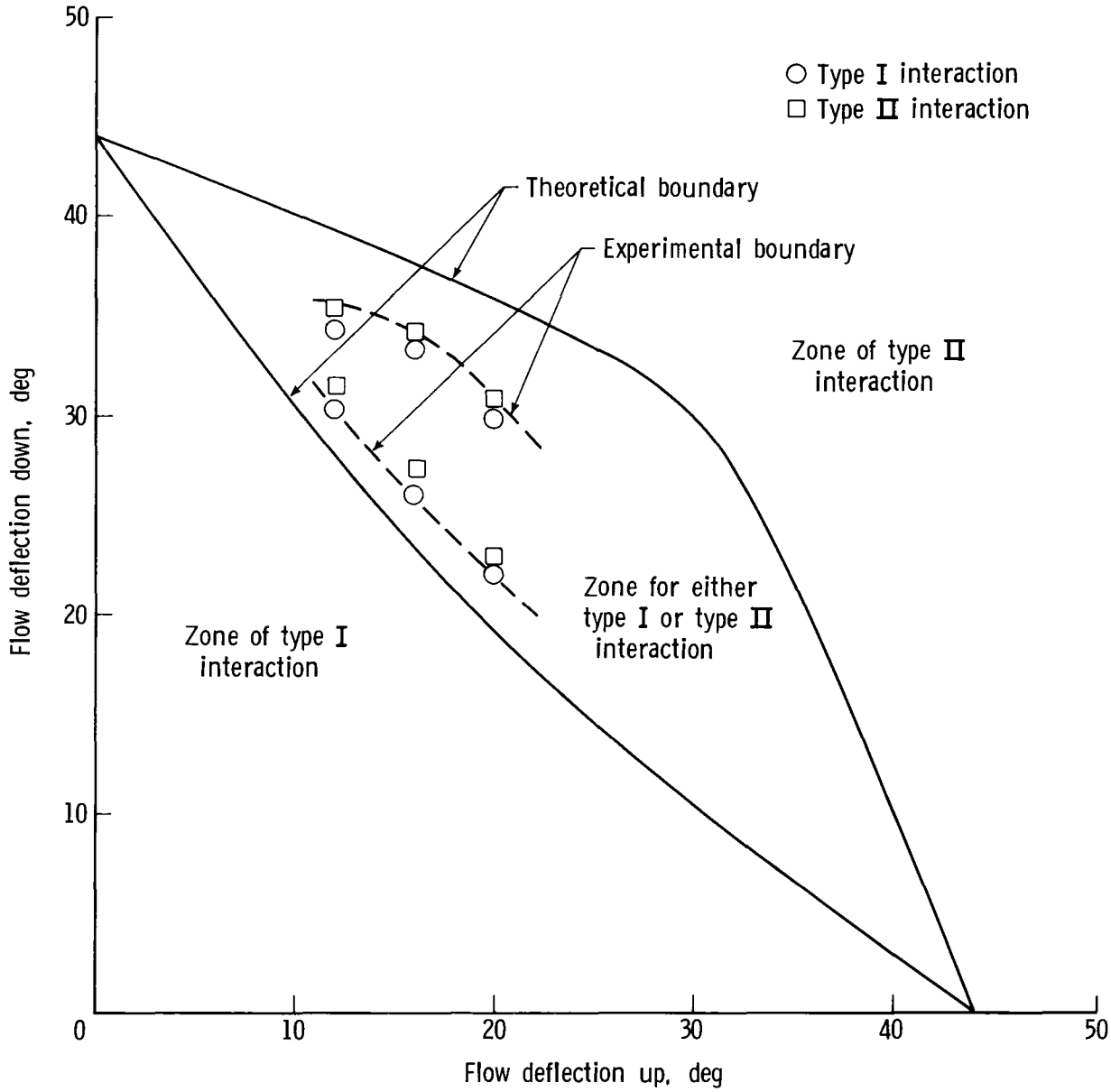

Figure 16.- Comparison of theoretically and experimentally determined boundaries of zone where either type I or type II interaction occurs at Mach 10.

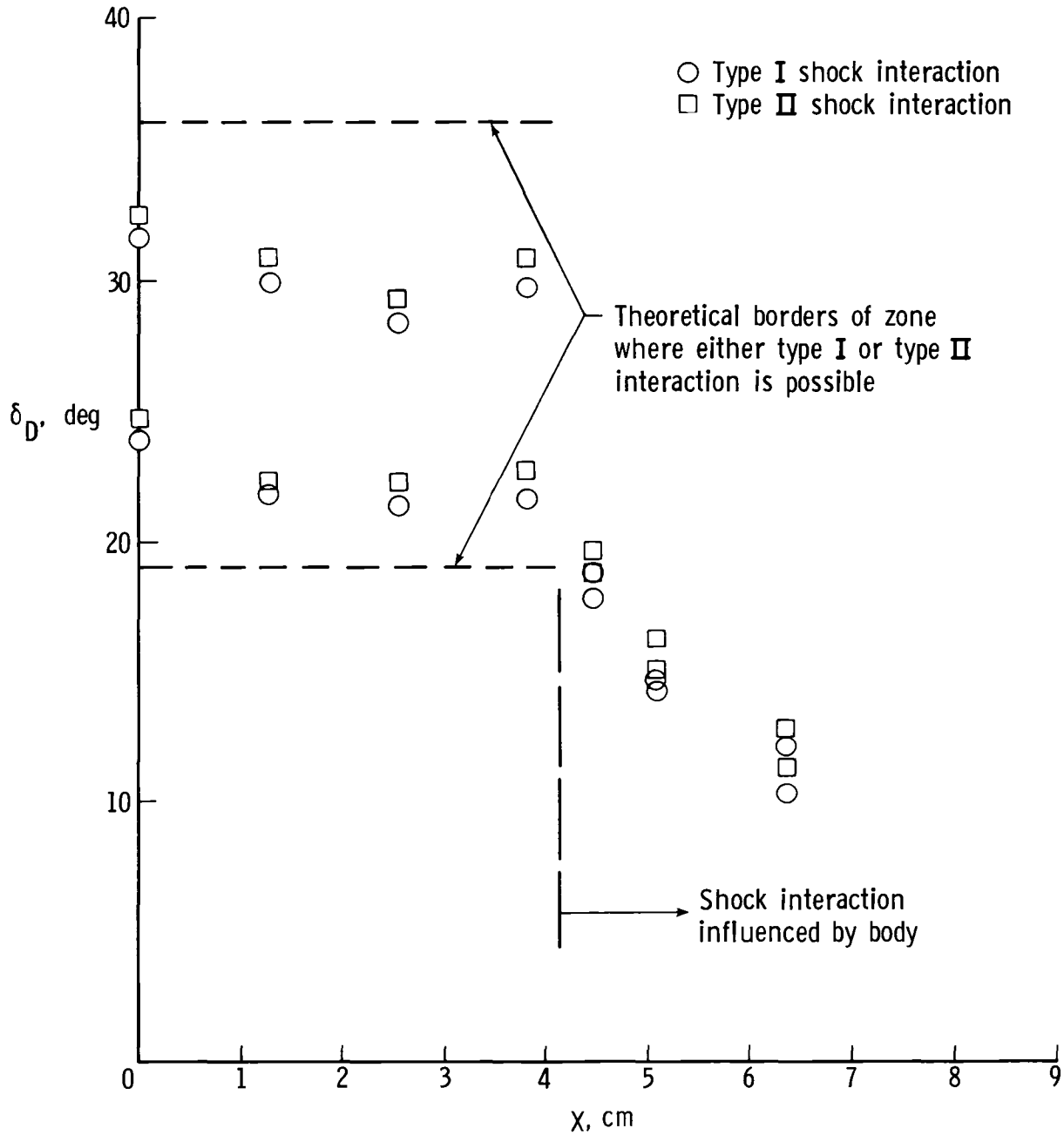

(a) $\delta_U = 20^o$.

Figure 17.- Experimental analysis of body angles where either type I or type II interaction is possible. (See fig. 14.)

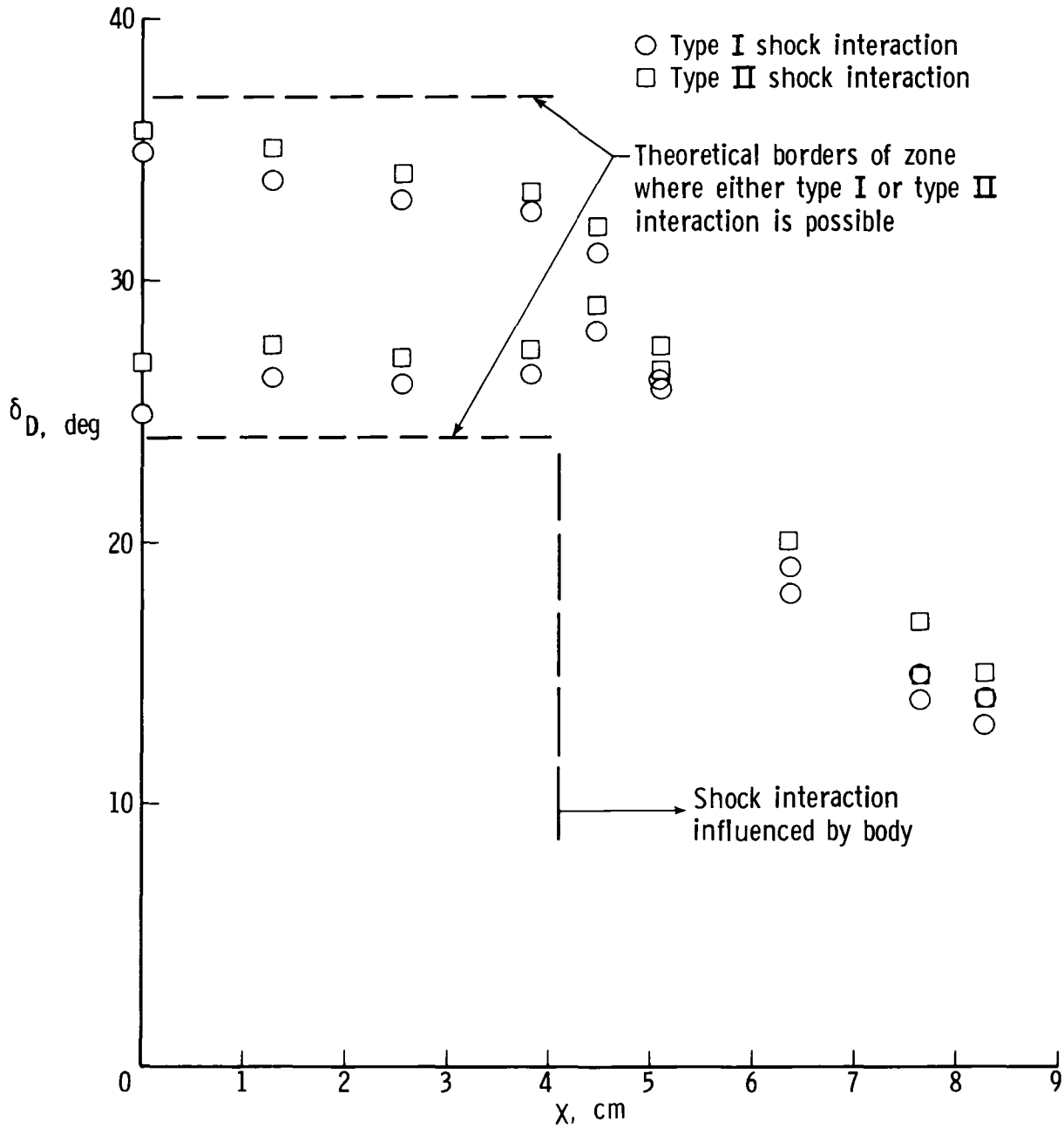

(b) $\delta_U = 16^o$.

Figure 17.- Continued.

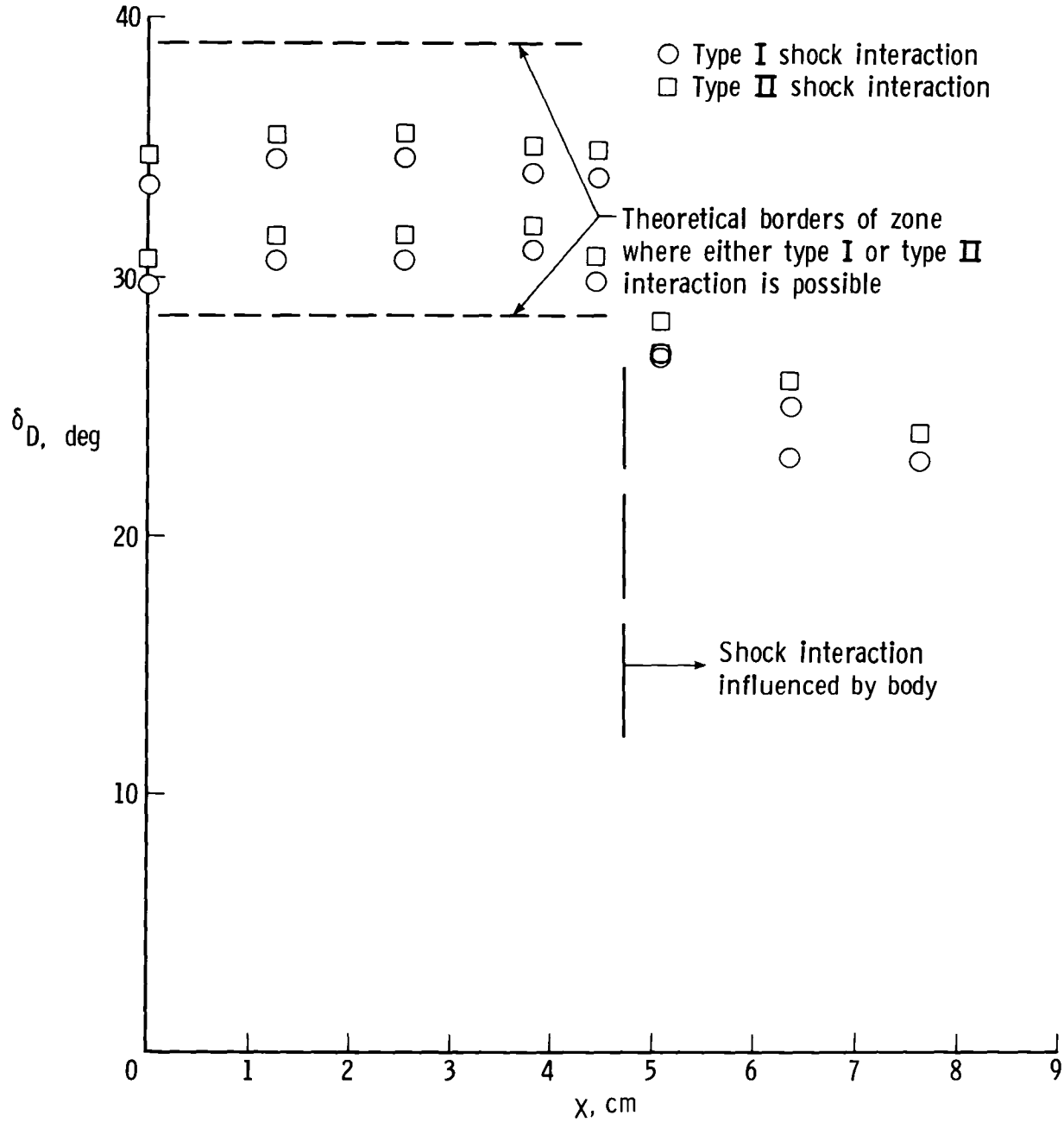

(c) $\delta_U = 12^o$.

Figure 17.- Concluded.

End of Document